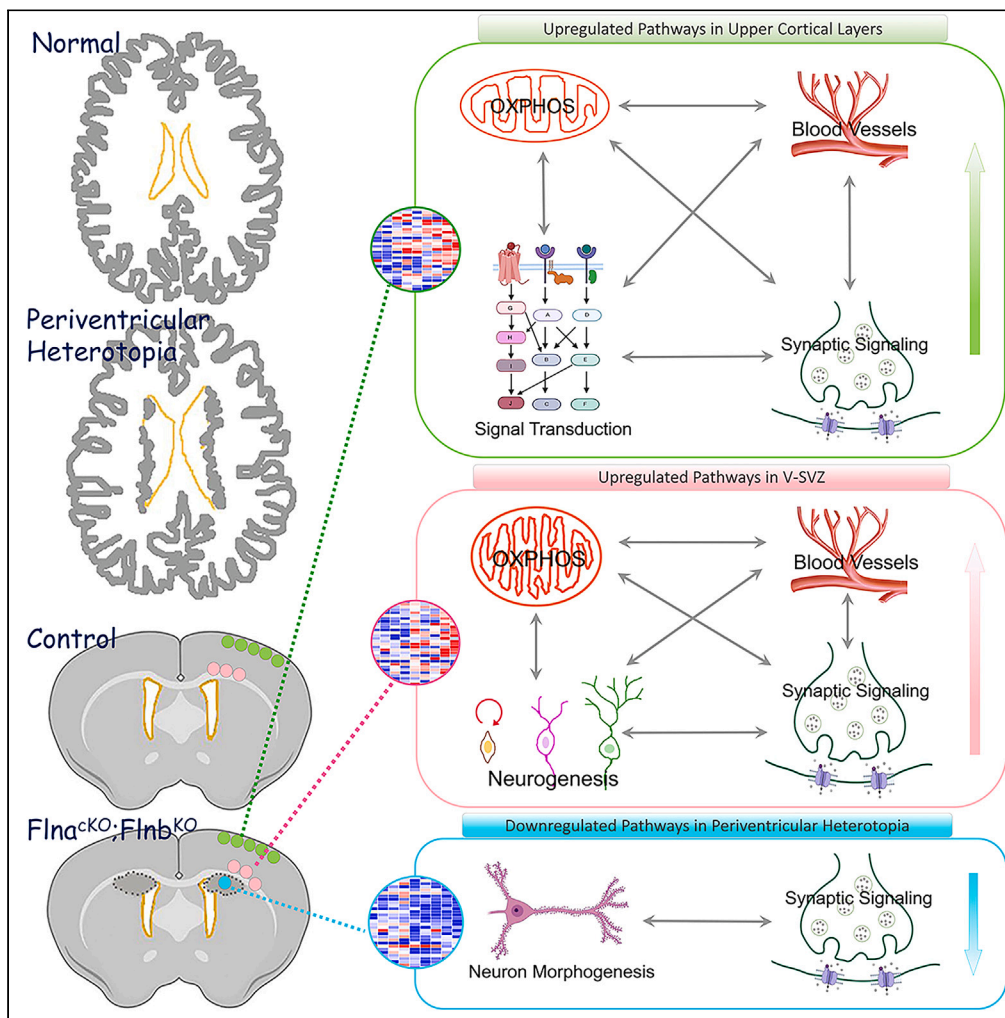Article

Sustained generation of neurons destined for neocortex with oxidative metabolic upregulation upon filamin abrogation

Caroline A.
Kopsidas, Clara C.
Lowe, Dennis P.
McDaniel,
Xiaoming Zhou,
Yuanyi Feng

yuanyi.feng@usuhs.edu

Highlights

A mouse model of
periventricular heterotopia
shows neurogenesis in
adult V-SVZ

Adult-made neurons share
transcriptome profiles with
neurons in upper
neocortex

Elevated V-SVZ activity is
coupled with aerobic ATP
synthesis and
vascularization

Neurogenesis in adulthood
is associated with brain
system-wide vitalization

Article

Sustained generation of neurons destined for neocortex with oxidative metabolic upregulation upon filamin abrogation

Caroline A. Kopsidas,[1,4,6] Clara C. Lowe,[1,4,7] Dennis P. McDaniel,[2] Xiaoming Zhou,[3] and Yuanyi Feng[1,5,8,*]

SUMMARY

Neurons in the neocortex are generated during embryonic development. While the adult ventricular-sub-ventricular zone (V-SVZ) contains cells with neural stem/progenitors' characteristics, it remains unclear whether it has the capacity of producing neocortical neurons. Here, we show that generating neurons with transcriptomic resemblance to upper layer neocortical neurons continues in the V-SVZ of mouse models of a human condition known as periventricular heterotopia by abrogating Flna and Flnb. We found such surplus neurogenesis was associated with V-SVZ's upregulation of oxidative phosphorylation, mitochondrial biogenesis, and vascular abundance. Additionally, spatial transcriptomics analyses showed V-SVZ's neurogenic activation was coupled with transcriptional enrichment of genes in diverse pathways for energy metabolism, angiogenesis, cell signaling, synaptic transmission, and turnovers of nucleic acids and proteins in upper cortical layers. These findings support the potential of generating neocortical neurons in adulthood through boosting brain-wide vascular circulation, aerobic adenosine triphosphate synthesis, metabolic turnover, and neuronal activity.

INTRODUCTION

Neurons in the cerebral cortex are generated during embryogenesis following a precisely orchestrated developmental program. This program ensures both the timely production of cortical excitatory neurons from neural stem/progenitor cells (NSPCs), in the dorsal ventricular-subventricular zone (V-SVZ) situated adjacent to the brain ventricles, and the subsequent radial migration of newborn neurons to form laminated neocortex underneath the brain surface.[1–4] With sufficient neurons being made to sustain cortical function throughout life, NSPCs turn off neurogenesis and switch to making astrocytes and oligodendrocytes to support neuronal function.[5–7] This NSPC fate-switch occurs before birth in both humans and rodents. Although cell proliferation persists in V-SVZ of juvenile and adult brains of humans, primates, and rodents,[8–10] evidence for neurogenic capacities in the postnatal and adult V-SVZ is limited to producing olfactory neurons in rodents.[11–14] As olfaction is less pivotal for sensory input in humans than rodents, it remains unclear whether cortical neurons can be made in adulthood to have an impact on human brain function or disorders. Thus, suitable experimental models and direct evidence are necessary to determine the propensity, mechanisms, and the functional implications of neurogenesis in the adult V-SVZ.

By studying the human brain developmental disorder periventricular heterotopia (PH) through murine models of Flna loss of function (LOF), we have shown previously that a "surplus" population of neurons can be made independent of embryonic neocortical neurogenesis and neuronal migration.[15] PH, also known as periventricular nodular heterotopia or subependymal gray matter heterotopia, is a brain malformation characterized by abnormal clumping of isolated or confluent neuronal nodules along the wall of lateral ventricles.[16–18] Although many PH cases are sporadic, LOF mutations of the X-linked gene *FLNA* account for 20%–30% of instances.[19–23] The affected individuals with *FLNA* mutations are mostly females; males in the pedigree may be affected but are often aborted spontaneously, presumably due to cardiovascular defects.[18,24,25] The most notable neurological symptom of PH is developing epilepsy beginning in mid-adolescence.[22,26–28] Although some affected individuals may present mild cognitive, behavioral, or reading deficits,[29–31] the condition can often be asymptomatic or associated with little or no impairments on intellectual abilities.[20–23,32,33] In line with the minimal cognitive deficits, alterations in neocortical structures of the affected brains are often insignificant despite the presence of a large number of periventricular ectopic neurons,[29,34–37] though a recent report of whole-brain multimodal MRI study suggested an association of PH with cortical thickening.[38] Overall, the generation

---

of periventricular neurons has minimal or very mild impairments to canonical developmental programs for neocortical neurogenesis and neuronal migration.

FLNA encodes a 280 kDa protein filamin A (FLNa) and is joined by *FLNB* and *FLNC* to form the filamin family.[39–41] While the expression of *FLNC* is specific to skeletal, cardiac, and smooth muscles, *FLNA* and *FLNB* are both expressed ubiquitously. The three filamin proteins share a similar structure including an N-terminal actin-binding domain, two hinge domains, 24 immunoglobulin-like (Ig-like) repeats, and a C-terminal dimerization domain, allowing filamins to crosslink actin filaments as homo- or heterodimers.[42–44] Besides actin, filamins have been reported to interact through the Ig-like repeats with over a hundred proteins. These filamin interacting proteins have diverse functions in cell surface, cytoplasm, and the nucleus,[45–49] suggesting multifaced roles of filamins in cell signaling, gene expression, and homeostasis besides actin stabilization. Although PH is traditionally regarded as a neuronal migration disorder caused by mosaic *FLNA* expression in heterozygous females, it does not explain cases caused by germline *FLNA* mutations in males,[25,32,34,50–53] which argue against a simple migratory incompetence of FLNA-deficient neurons. While the migration defect of *FLNA* LOF may be masked by *FLNB*, our mouse model of Flna and Flnb double LOF in NSPCs showed high penetrance of PH without affecting neocortical neuronal migration and lamination.[15] Instead, we showed that periventricular neurons were made extraneously due to altered V-SVZ microenvironment resulting from epithelium mesenchymal transition (EMT) of polarized radial glial progenitors with filamin deficiency. EMT is a process that entails profound change in cellular phenotype and tissue microenvironment. It was elevated in filamin-deficient V-SVZ due to compromised attenuation of IgF and Vegf signaling between NSPCs and nascent cerebral blood vessels in mid gestation, leading to feedforward escalation of both angiogenesis and neurogenesis. As a result, periventricular neuronal nodules were associated with increased vascular abundance, becoming first detectable at birth but continuing to grow postnatally.[15] This timeline of periventricular heterotopia development in filamin mutant mice agrees with the corresponding human condition, in which neuronal nodules could be seen before birth but usually become evident along with the onset of epileptic seizures in the second decade of life. These together suggest strongly that PH is a condition occurring independent of canonical neocortical neurogenesis, in which a surplus of neurons is generated in the late-embryonic and postnatal V-SVZ.

Consistent with a vascular input in PH initiation shown by filamin-deficient mice, *FLNA* mutations often cause cardiovascular defects.[15,23,25,54–56] This is intriguing as blood vessels are considered a major neurogenic niche in the V-SVZ of adult mammalian brains.[57,58] Apart from supplying oxygen and nutrients for brain energy metabolism, cells of the vasculature can secrete VEGF and other factors to promote NSPCs neurogenesis.[59–62] Thus, with a microenvironment of abundant blood vessels in the V-SVZ, filamin-deficient NSPCs may fail to turn off the production of neurons after the pre-programmed window of cortical neurogenesis and neuronal migration, resulting in continued generation of neurons destined for the neocortex in the dorsal V-SVZ after birth and the formation of heterotopic neuronal nodules locally.

In this study, we set out to further test the hypothesis that PH results from noncanonical neocortical neurogenesis by determining (1) whether the generation of neocortical neurons persists in the postnatal and adult V-SVZ in mouse models of PH, (2) what constitutes the molecular networks underlying sustained production of periventricular neurons, and (3) how neurons in periventricular nodules are distinctive compared to neurons in the neocortex. Our data demonstrate that filamin deficiency results in PH with combined upregulations of neocortical vascular abundance, oxidative energy production, diverse cell signaling pathways, and expression of neuronal activity genes. Such brain-wide metabolic activation may underlie the generation of neurons with transcriptome resemblance to neurons of the upper cortical layers in the postnatal and adult V-SVZ. These results provide a conceptual possibility of boosting V-SVZ neurogenesis by targeting FLNA to enhance vascular circulation and energy metabolism at the brain systems level.

RESULTS

Neurons in periventricular heterotopia increase continuously in juvenile and adult Fln[KO] mice

Our previous developmental analyses have shown that mice with Flna null mutation die by embryonic day 15 (E15) with severe cardiovascular defects, whereas mice with NSPC conditional Flna deletion mediated by the Emx1-Cre or the Nes8-Cre driver (referred to as Flna[cKO] mice) survive with little brain anatomical aberrations.[15,55] However, when we introduced Flnb mutations to Flna[cKO] mice, PH, defined by the presence of ectopic neurons (NeuN[+]) along the wall of lateral ventricles on both sides of the brain, was found in all mice with compound Flna[cKO] and Flnb homozygous mutations (Flna[f/yCre+]; Flnb^{−/−} males or Flna[f/f Cre+]; Flnb^{−/−} females, referred to as Fln[KO] or PH mice collectively hereafter). About 20% of mice with compound Flna[cKO] and heterozygous Flnb mutations (Flna[f/yCre+]; Flnb^{+/−} males or Flna[f/fCre+]; Flnb^{+/−} females) were also found to present bilateral PH with similar developmental and brain anatomical phenotype. In all cases, PH becomes detectable at perinatal ages.[15] To better assess the X-linked mosaicism, we also examined a set of female mice with compound heterozygous Flna[cKO] and homozygous Flnb mutations (Flna[f/wt Cre+]; Flnb^{−/−}). Similar to females with heterozygous *FLNA* LOF in the human condition, female mice with mosaic NSPC Flna conditional and Flnb null mutations exhibited bi-lateral periventricular neuronal nodules with 100% penetrance, whereas Flnb abrogation alone (Flna[f/f Cre−]; Flnb^{−/−} females or Flna[f/y Cre−]; Flnb^{−/−} males) was not found to cause neuronal heterotopia or other brain structural changes (Figures 1A, S1A, and S1B). Immuno-histological (IH) analyses showed that Flna was predominantly expressed in NSPCs of both embryonic, postnatal, and adult V-SVZ as well as in cerebral blood vessels. It was effectively deleted along with Flnb in the neuroparenchyma of developing, postnatal, and adult brains in Fln[KO] mice without affecting its vascular expression (Figures 1B–1D, S1C, and S1F). This suggests that the major role of Flna in the neuroparenchyma lies in NSPCs of the V-SVZ where Flna and Flnb form heterodimers and function together.[44] These findings support the validity of using Fln[KO] mice to model the human PH condition.

The continued expression of Flna in NSPCs of the postnatal and adult V-SVZ suggested that Flna's function extends beyond embryonic development. In line with the fact that PH was initiated by NSPC defects that led to extraneous neurogenesis, we found that periventricular neuronal nodules in Fln[KO] mice grew continuously during not only neonatal development but also young adulthood. By following a cohort of
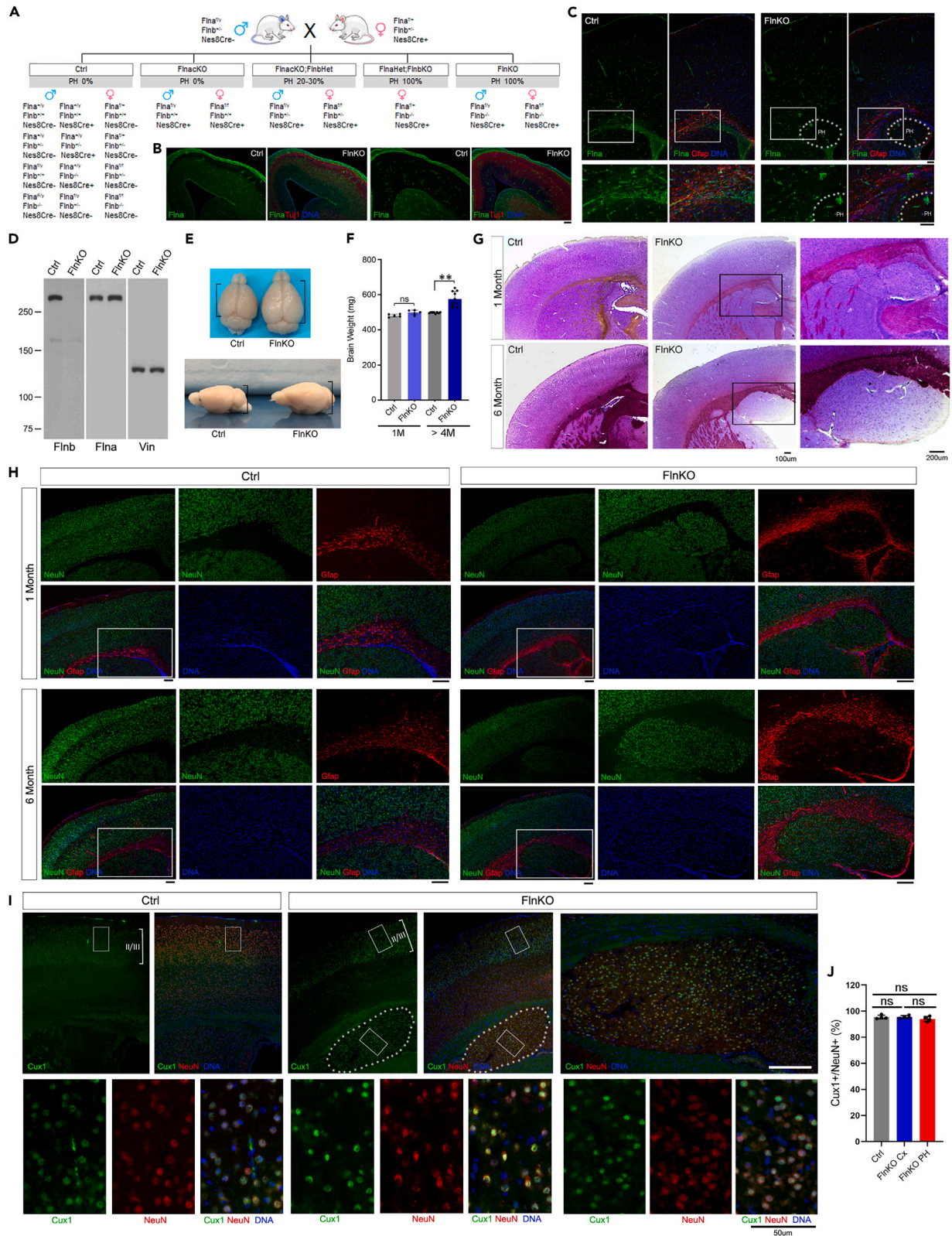
Figure 1. Periventricular heterotopia continue to grow in Fln^{KO} mice after weaning

(A) A breeding scheme for generating mice with single and double mutations of Flna and Flnb as well as the genetic penetrance of PH in filamin mutant mice.

(B) Representative images of embryonic cortical sections (E14.5) double immunostained with antibodies against Flna (green) and Tuj1 (red). Nuclear DNA was stained with Hoechst 33342 and shown in blue. Note the specific deletion of Flna in cortical NSPCs and neurons of Fln^{KO} mice by Nes8Cre.

(C) Representative images of cortical sections of weaning age Fln^{KO} and control mice that were double immunostained with antibodies against Flna (green) and Gfap (red). Nuclear DNA was stained with Hoechst 33342 and shown in blue. Note Flna's presence in the V-SVZ and cerebral blood vessels of control mice and its specific absence in the V-SVZ of Fln^{KO} mice.

(D) Flna and Flnb immunoblots of cortical total protein exacts from control and Fln^{KO} mice at 4 months of age. Note the presence of Flna in Fln^{KO} cortices, which is presumably from cerebral blood vessels.

(E) Representative brain images of a Fln^{KO} and a control mouse at 10 months of age.

(F) Brain weights of Fln^{KO} and control mice at ages of weaning (1M) and 4 months or older ($\geq$4M), respectively. Shown are mean $\pm$ SD. **$p < 0.005$ by Student's t test.

(G) Representative images of Cresyl-violet-stained brain sections of a Fln^{KO} and control mice at weaning (1 month) and 6 months of age, respectively. High-magnification images of boxed regions are included.

(H) Representative images of NeuN (green) and Gfap (red) double immunostained brain sections of Fln^{KO} and control mice at weaning (1 month) and 6 months of age, respectively. Nuclear DNA was stained with Hoechst 33342 and shown in blue. High-magnification images of boxed regions are included.

(I) Representative images of NeuN (red) and Cux1 (green) double immunostained brain sections of Fln^{KO} and control mice at 4 months of age. Nuclear DNA was stained with Hoechst 33342 and shown in blue. High-magnification images of boxed regions are included. The position of PH is marked by dotted lines.

(J) Quantification (%) of Cux1+ neurons in neocortical layer II/II (bracketed upper cortical layers) of control or Fln^{KO} mice or in periventricular heterotopia (PH). Shown are mean $\pm$ SD of n = 4 biological replicates.

Scale bars: 100 μm or as indicated.

See also Figure S1.

Fln^{KO} mice and their littermate control mice from weaning to 10 months of age, we found that the brain weight of Fln^{KO} mice, while comparable to that of control mice at weaning age, became significantly greater after young adulthood at ages approximately 4 months or older (Figures 1E and 1F). In brains of these mature Fln^{KO} mice, periventricular nodules were heterogeneous in size and shape and frequently grew together, forming larger masses or band-like structures with diameters comparable to the thickness of the overlying neocortex. Nonetheless, cerebral cortical size and neuronal lamination were overall indistinguishable between Fln^{KO} and control brains[15] (Figures 1G and 1H). Although the nodular mass may disrupt ventricular ependyma and obstruct ventricular circulation to cause hydrocephalus that contributes to enlarged appearance of Fln^{KO} brains, hydrocephalus was only seen in less than half of mutant mice and did not account for the net gain in brain weight from weaning to midlife. Thus, these data suggest that Flna LOF in postnatal and adult NSPCs resulted in progressive addition of neurons to periventricular nodules.

We found periventricular neuronal nodules, regardless of size and distribution, were exclusively surrounded by glial fibers with high level of Gfap (Figures 1C–1H, S1G, and S1H). Gfap is an intermediate filament protein expressed by a subpopulation of astrocytes that are derived from embryonic NSPCs and retain the potential of generating neuroblasts in the adult V-SVZ.[9,62] Interestingly, the immunoreactivity of Gfap showed a substantial overlap with that of Flna in the V-SVZ of juvenile and adult brains, and it is not only enhanced around periventricular neurons but also found inside of the nodular mass (Figures 1C and 1H). A majority of periventricular neurons expressed Cux1, a marker for excitatory neurons in upper cortical layer II/III generated toward the end of embryonic cortical neurogenesis (Figure 1I). This shared cell molecular identity between periventricular and late-born neurons in the upper cortex, combined with the local increase in Gfap$^+$ cells, suggested that NSPCs with Flna and Flnb double LOF failed to shutdown neurogenesis at the end of embryonic development and remained active in the postnatal and adult V-SVZ. The olfactory bulbs in Fln^{KO} mice were of normal size and structure (Figures 1E, S1I, and S1J), which further suggests that periventricular neurons were not migration-arrested olfactory neurons associated with the rodent-specific V-SVZ neurogenesis. Instead, they were likely cortical neurons produced by NSPCs that retained neurogenic propensity in the V-SVZ of postnatal and adult Fln^{KO} mice.

Increased stemness and cellular activities in the V-SVZ of Fln^{KO} mice

To obtain further evidence for sustained generation of neocortical neurons in adult Fln^{KO} mice, we examined cellular compositions and activities adjacent to periventricular neuronal nodules. Besides Gfap, we found neurons in the nodular mass along the ventricular wall were surrounded by clusters of cells expressing the proliferation antigen Ki67 or the neuroblast marker Dcx (Figures 2A–2D and S2A). Although these markers for stemness and neurogenesis were also detectable in the V-SVZ of control mice, their abundance were remarkably higher around periventricular neurons. Furthermore, we found cells in the V-SVZ of Fln^{KO} mice proliferate much more actively than those in control mice as evidenced by significant increases in EdU incorporation (Figures 2E–2G and S2B). Notably, EdU$^+$ cells in Fln^{KO} V-SVZ are distributed around periventricular neurons along with cells expressing Gfap or Dcx. This suggests that Fln^{KO} NSPCs' proliferative and neurogenic activities were beyond the routine olfactory neurogenesis and largely dedicated toward generating periventricular neurons. Along with this notion, cells expressing Olig2 and Sox10, which mark oligodendrocytes and precursors, were also significantly elevated in the V-SVZ of Fln^{KO} compared to that of control mice (Figures 2H–2K, S2C, and S2D). Such complementary increase in periventricular neurogenic and oligodendrocyte differentiation indicates there were coordinated upregulation in stemness and cellular activities toward generating both neurons and their supporting cells in the V-SVZ of Fln^{KO} mice.
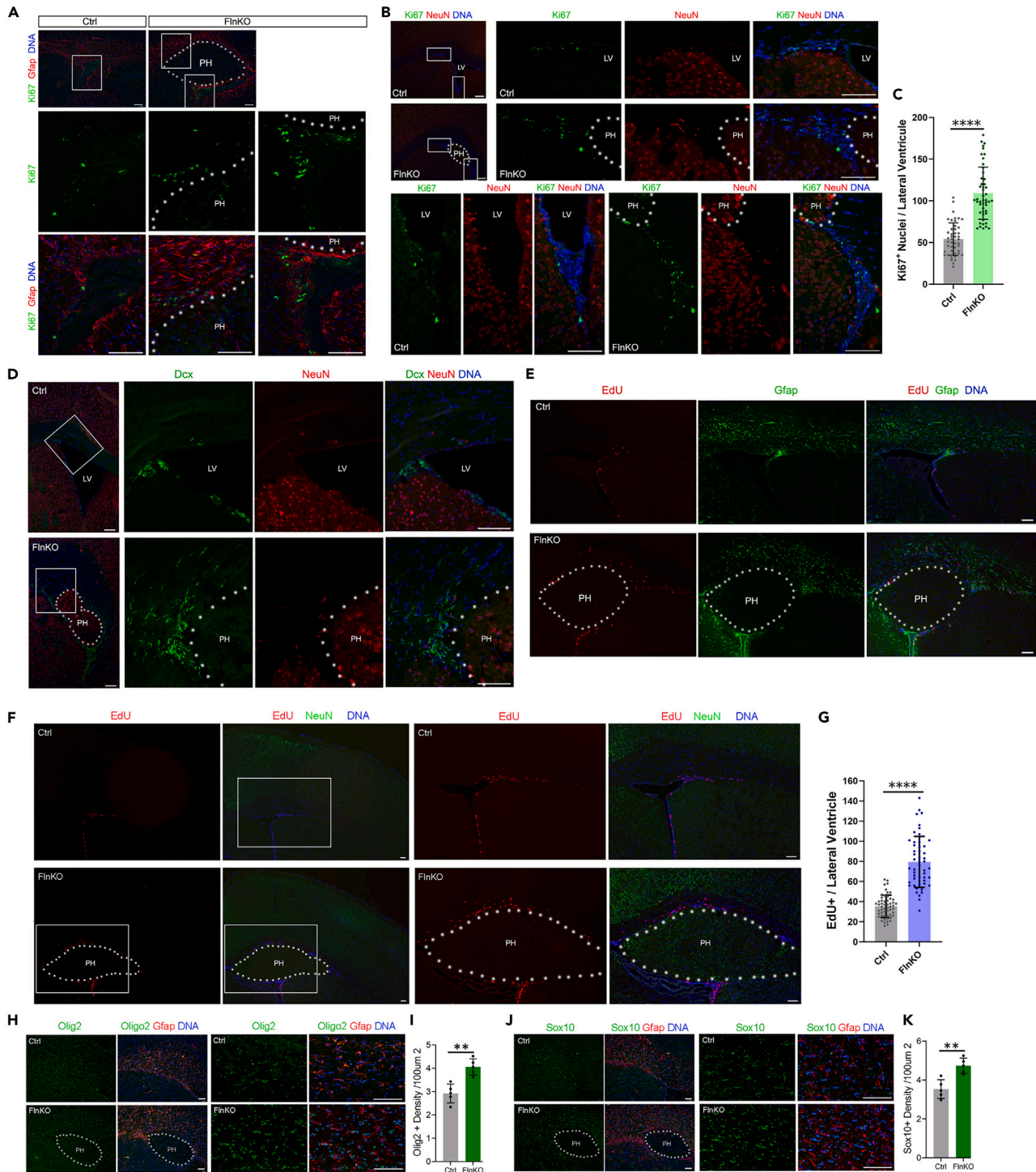
Figure 2. Increased stemness and cellular activity toward neurogenesis and glial differentiation in the V-SVZ of Fln^KO mice

(A) Representative images of Ki67 (green) and Gfap (red) double immunostained brain sections of Fln^KO or control mice at 4 months of age. Nuclear DNA was stained with Hoechst 33342 and shown in blue. High-magnification images of boxed regions are included. The position of PH is marked by dotted lines.

(B) Representative images of Ki67 (green) and NeuN (red) double immunostained brain sections of Fln^KO or control mice at 4 months of age. Nuclear DNA was stained with Hoechst 33342 and shown in blue. High-magnification images of boxed regions are included. The position of PH is marked by dotted lines.

(C) Quantification of Ki67+ cells in Fln^KO or control mice at 3–4 months of age. Shown are total Ki67+ nuclei near the entire lateral ventricular area on each brain section (*n* = 4 biological replicates). ****p < 0.0001 by Student's t test.

Figure 2. Continued

(D) Representative images of DCX (green) and NeuN (red) double immunostained brain sections of Fln^{KO} or control mice at 3 months of age. Nuclear DNA was stained with Hoechst 33342 and shown in blue. High magnification images of boxed regions are included. The position of PH is marked by dotted lines.

(E) Representative images of brain sections of Fln^{KO} or control mice at 3 months of age that were stained by EdU (red) and immunostained by anti-NeuN (green). Nuclear DNA was stained with Hoechst 33342 and shown in blue. The position of PH is marked by dotted lines.

(F) Representative images of brain sections Fln^{KO} or control mice at 3 months of age that were stained by EdU (red) and immunostained by anti-Gfap (green). Nuclear DNA was stained with Hoechst 33342 and shown in blue. High-magnification images of boxed regions are included. The position of PH is marked by dotted lines.

(G) Quantification of EdU+ cells in Fln^{KO} or control mice at 3–4 months of age. Shown are total EdU+ nuclei near the entire lateral ventricular area on each brain section ($n = 3$ biological replicates). ****$p < 0.0001$ by Student's t test.

(H) Representative images of Olig2 (green) and Gfap (red) double immunostained brain sections of Fln^{KO} or control mice at 3 months of age. Nuclear DNA was stained with Hoechst 33342 and shown in blue. The position of PH is marked by dotted lines.

(I) Quantification of the density of Olig2+ cells in the dorsal V-SVZ of Fln^{KO} or control mice. Shown are Mean $\pm$ SD. **$p < 0.005$ by Student's t test.

(J) Representative images of Sox10 (green) and Gfap (red) double immunostained brain sections of control or Fln^{KO} mice at 3 months of age. Nuclear DNA was stained with Hoechst 33342 and shown in blue. The position of PH is marked by dotted lines.

(K) Quantification of the density of Olig2+ cells in the dorsal V-SVZ of Fln^{KO} or control mice. Shown are mean $\pm$ SD. **$p < 0.005$ by Student's t test.

Scale bars: 100 μm or as indicated.

See also Figure S2.

Upregulation of genes mediating both neurodevelopment and oxidative phosphorylation in Fln^{KO} V-SVZ

To determine the molecular basis and functional gene networks associated with periventricular neurogenesis at the brain systems level, we employed spatial transcriptomics to capture regional specific gene expression profiles. We prepared brain sections from Fln^{KO} and control mice at 3 months of age ($n = 3$ each) and double stained them with fluorescent-conjugated antibodies to Gfap and NeuN. Guided by Gfap signals along the lateral ventricles, we selected 16 and 15 regions of interest (ROIs) from the dorsal V-SVZ of control and Fln^{KO} brains, respectively. Based on NeuN signals, we also selected 16 and 13 ROIs from upper cortical layers of control and Fln^{KO} brains, respectively. In addition, Gfap-NeuN double staining allowed the selection of 16 ROIs from the periventricular nodules of Fln^{KO} brains (Figure S3A). We used the NanoString GeoMx DSP platform, by which RNA-sequencing yielded expression data for 19,962 genes across all 76 sampled ROIs. Comparing regionally specific ROIs between Fln^{KO} and control mice revealed 4,003 and 7,411 differentially expressed genes (DEGs) in the V-SVZ and upper cortex, respectively. In addition, we identified 612 DEGs between ROIs in periventricular nodules and upper cortical layers of Fln^{KO} mice (Figures 3A and S3B–S3E). Therefore, despite the lack of discernible change in neocortical morphology, generation of periventricular neurons in Fln^{KO} mice was associated with remarkable transcriptome alterations in both V-SVZ and upper cortical layers.

To assess the molecular profile underling neurogenic activation in the V-SVZ of Fln^{KO} mice, we first queried DEGs identified across V-SVZ ROIs between Fln^{KO} and control mice. Out of the total 4,003 DEGs, the 1,489 downregulated DEGs showed no significant enrichments in pathway analysis. In contrast, the 2,514 upregulated DEGs in Fln^{KO} V-SVZ were found enriched in many functional pathways and biological processes, among which the KEGG pathway of oxidative phosphorylation (OXPHOS) was most significantly overrepresented (False Discovery Rate (FDR) = 1.2E-25; fold enrichment = 4.4) (Figure 3B). Remarkably, 65 of 133 genes participating in OXPHOS were upregulated in Fln^{KO} compared to control V-SVZ ROIs (Figures 3C and S4A), suggesting strongly that the increased V-SVZ stemness and neurogenic activities in Fln^{KO} mice were supported by elevating mitochondrial electron transport chain (ETC) function for aerobic ATP synthesis.

The GeoMx DSP data also indicated that transcriptional upregulations in mitochondrial oxidative metabolism were accompanied by increased expression of genes involving neural development and neuronal activities in the Fln^{KO} V-SVZ. Besides neurogenesis, the most significantly enriched BP terms of gene ontology (GO) analysis included vesicle-mediated transport in synapse, *trans*-synaptic signaling, neuron projection development, and neuron differentiation (Figure 3D). As 1,735 of DEGs upregulated across V-SVZ ROIs also showed significantly higher expression in upper cortical ROIs of Fln^{KO} mice (Figures 3A and S3E), we assessed the 779 genes that were exclusively upregulated in the Fln^{KO} V-SVZ to determine the V-SVZ-specific impact. Our pathway and GO enrichment analyses demonstrated that the V-SVZ-specific DEGs indeed overrepresented biological processes related to mitochondrial respiratory chain assembly, oxidative ATP metabolic processes, neurodevelopment, neuronal differentiation, as well as neuronal networking activities in synaptic signaling, transmission, and behaviors (Figures 3E and 3F). The neuronal-activity-related genes upregulated in the Fln^{KO} SVZ included molecules for synaptogenesis and synaptic signaling, such as Syn1, Syn2, Syngap1, Slitrk1, and Clstn2, as well as ion channels and glutamate receptors, such as Scn1b, Scn2b, Kcnc1, Grik5, and Gria1 (Figure 3G). For genes associated with neurodevelopment, significant upregulations occurred in diverse molecules that pose both extrinsic and intrinsic effects on neurogenesis and morphogenesis, such as Neurod2, a basic helix-loop-helix transcription factor that can induce neurogenic differentiation and maintain neuronal cell fate;[63] Ngfr, the receptor for nerve growth factor, which plays important roles in neuronal differentiation and survival; as well as Nrcam and Sema6b, which encode neuronal adhesion molecules for axon growth and guidance (Figure 3H). Overall, the transcriptome profile underlying increased neurogenesis in Fln^{KO} V-SVZ suggests co-upregulation of energy metabolism with activities toward neuronal differentiation. Such coordinated regulation of genes for mitochondrial function and neural development in the Fln^{KO} V-SVZ suggests that the switch of adult NSPCs from quiescence to neurogenesis and their commitment to neuronal differentiation require a metabolic upregulation to increase the efficiency of ATP synthesis by OXPHOS.

To validate the co-upregulation of V-SVZ neurogenesis with energy metabolism implicated by the GeoMx DSP data, we first performed IH analyses of NeuroD2 and mitochondrial respiratory complex I. In line with a sufficient role of NeuroD2 in inducing neurogenesis,[63] we found NeuroD2's immunoreactivity was much stronger in the V-SVZ of adult Fln^{KO} mice than that of the control mice (Figure 3I). Respiratory complex
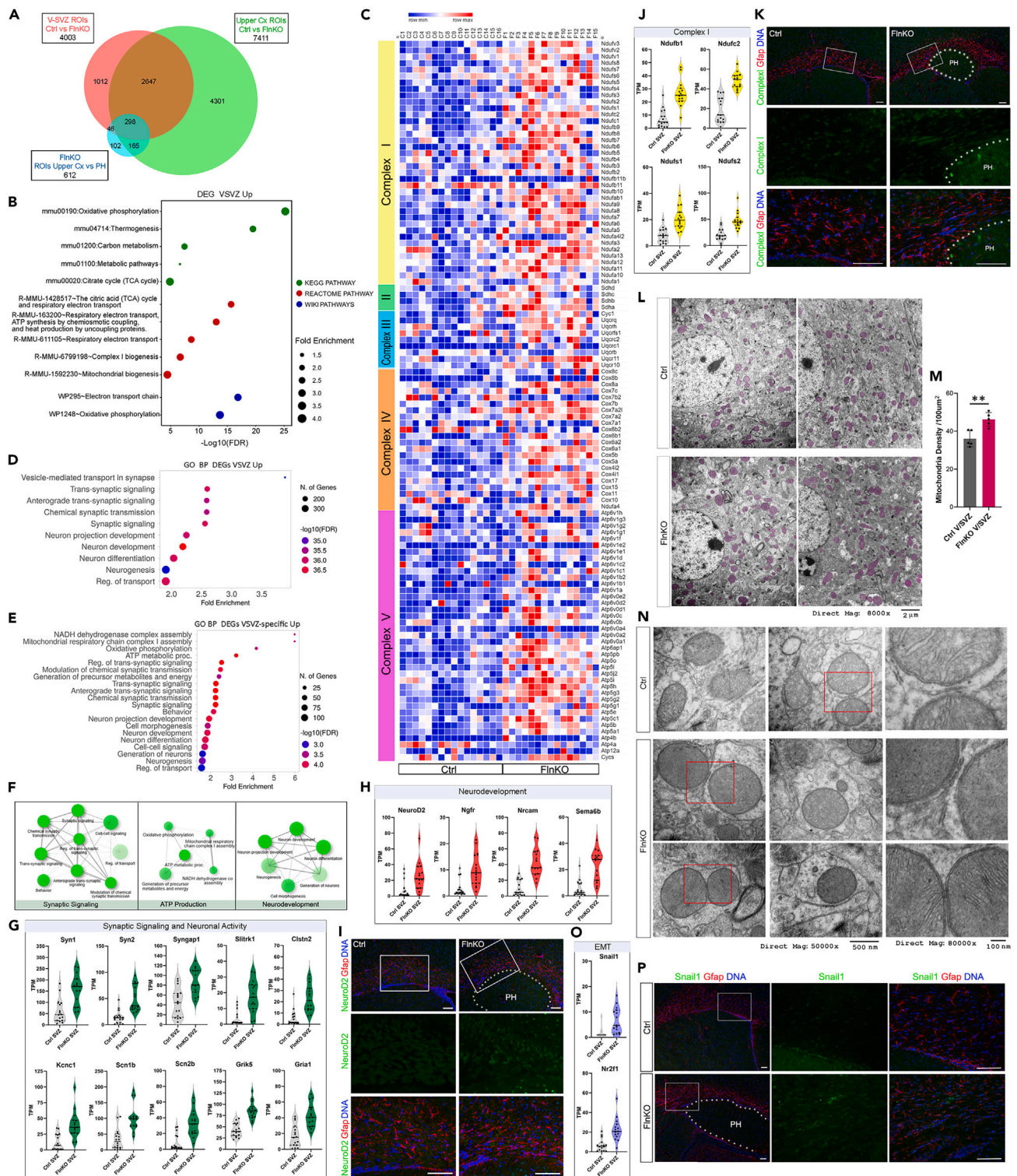
Figure 3. Increased V-SVZ neurogenesis in Fln^KO mice is associated with upregulation of oxidative phosphorylation and mitochondrial biogenesis

(A) Venn diagram of differentially expressed genes (DEGs) identified by GeoMx DSP analysis of mouse whole transcriptome. A total of 76 regions of interests (ROIs) representing V-SVZ, upper cortical layers, and periventricular heterotopia were analyzed in Fln^KO and control mice at 3–4 months of age (biological replicate = 3 each). Shown are numbers of DEGs from V-SVZ ROIs between Fln^KO and control mice, from upper cortical ROIs between Fln^KO and control mice, and between periventricular heterotopia (PH) ROIs and upper cortical layer ROIs of Fln^KO mice.

Figure 3. *Continued*

(B) Summary of KEGG, Reactome, and Wiki pathway enrichment analyses of upregulated DEGs across V-SVZ ROIs of Fln[KO] mice compared to those of control mice.

(C) Heatmap representation of the level of nuclear encoded genes of mitochondrial ETC complexes expressed in V-SVZ ROIs of Fln[KO] and control mice.

(D) Gene Ontology biological processes (BP) terms enriched in upregulated DEGs across V-SVZ ROIs of Fln[KO] mice compared to those of control mice.

(E) Gene Ontology biological processes (BP) terms enriched in DEGs exclusively upregulated across V-SVZ ROIs of Fln[KO] mice compared to those of control mice.

(F) Network plots show the relationship of enriched BP terms shown in (E).

(G) Expression levels (transcripts per million/TPM) of selected neuronal activity genes that were significantly upregulated across V-SVZ ROIs of Fln[KO] mice relative to those of control mice.

(H) Expression levels (transcripts per million/TPM) of selected neurodevelopmental genes that were significantly upregulated across V-SVZ ROIs of Fln[KO] mice relative to those of control mice.

(I) Representative images of NeuroD2 (green) and Gfap (red) double immunostained brain sections of Fln[KO] or control mice at 3 months of age. Nuclear DNA was stained with Hoechst 33342 and shown in blue. High-magnification images of boxed regions are included. The position of PH is marked by dotted lines.

(J) Expression levels (transcripts per million/TPM) of selected ETC complex I genes that were significantly upregulated across V-SVZ ROIs of Fln[KO] mice relative to those of control mice.

(K) Representative images of the Ndufs1 subunit of complex I (green) and Gfap (red) double immunostained brain sections of Fln[KO] or control mice at 3 months of age. Nuclear DNA was stained with Hoechst 33342 and shown in blue. High-magnification images of boxed regions are included. The position of PH is marked by dotted lines.

(L) Representative electron micrographs of cortical V-SVZ of Fln[KO] and control mice at 5 months of age. Mitochondria are highlighted in mauve.

(M) Quantification of mitochondrial density in the soma of V-SVZ cells of Fln[KO] and control mice at 5 months of age. Shown are mean ± SD. **$p < 0.005$ by Student's t test.

(N) Representative electron micrographs of mitochondria in V-SVZ of Fln[KO] and control mice at 5 months of age. High-magnification images of boxed areas are included.

(O) Expression levels (transcripts per million/TPM) of EMT inducers Snail 1 and Nr2f1 that were significantly upregulated across V-SVZ ROIs of Fln[KO] mice relative to those of control mice.

(P) Representative images of Snail1 (green) and Gfap (red) double immunostained brain sections of Fln[KO] or control mice at 3 months of age. Nuclear DNA was stained with Hoechst 33342 and shown in blue. High-magnification images of boxed regions are included. The position of PH is marked by dotted lines.

Scale bars: 100 μm or as indicated.

See also Figures S3 and S4.

I is the first enzyme of the ETC containing 45 subunits, of which 38 are produced by the nuclear genome. We found that of the 38 nuclear transcripts of complex I, 28 were upregulated in the Fln[KO] V-SVZ (Figures 3C, 3J, and S4A). Correlated with increased complex I transcripts, Ndufs1, known as the 75 kDa subunit of complex I, showed stronger immunoreactivities in the Fln[KO] V-SVZ (Figure 3K), suggesting that the elevation in multiple complex I transcripts reflected increased mitochondria biogenesis. To confirm this, we performed transmission electron microscopic analysis to determine the mitochondrial density and ultrastructure in the V-SVZ. We found that despite heterogeneity in size, morphology, and distribution, mitochondria in the V-SVZ of Fln[KO] mice were not only significantly higher in density compared to those in the V-SVZ of control mice but also showed distinctive structural features (Figures 3L–3N). These mitochondria frequently displayed a spherical shape containing densely packed cristae (Figure 3N). While the spherical morphology is a characteristic of mitochondria in stem cells, condensed mitochondrial cristae indicate strong ETC activities for ATP synthesis.[64,65] These data further support the notion that generation and functional maturation of new neurons in the V-SVZ of Fln[KO] mice rely on a metabolic upgrade from anaerobic glycolysis to OXPHOS through mitochondrial biogenesis. As ATP is highly indispensable for neuronal activities in the adult brain, our data imply that an essential task for neurogenesis in the postnatal and adult VSVZ is to fulfill the energy demand of neurons in the functional brain.

Notably, our GeoMx DSP analysis also revealed that Snai1, the master EMT inducer that drives the embryonic initiation of PH,[15] remained significantly upregulated in the adult Fln[KO] V-SVZ along with other EMT inducers, such as Nr2f1[66] (Figures 3O and 3P). This suggests that enhanced EMT resulting from filamin LOF persists to NSPCs in the postanal and adult V-SVZ, contributing to sustained neurogenesis.

Increased vascular abundance in Fln[KO] brains supports brain system-wide metabolic activation

The net effect of increased EMT in the embryonic Fln[KO] V-SVZ was elevations in both neurogenesis and angiogenesis.[15] In the adult brain, vascular circulation is essential for delivering glucose and oxygen to permit high-efficiency ATP synthesis by OXPHOS in order to support neuronal activities. Thus, it is possible that both EMT and energetics upregulation in adult Fln[KO] V-SVZ are associated with angiogenesis as observed in the developing Fln[KO] brain. Indeed, by quantifying the density of cerebral blood vessels and the level of vascular endothelial marker CD31, we found that the vascular abundance was significantly higher in Fln[KO] than in control cortices (Figures 4A–4D). Besides an overall increase in density, blood vessels in Fln[KO] brains, especially those surrounding and inside the periventricular nodules, frequently showed enlarged caliber (Figures 4A, 4B, and 4E). The large vessels near heterotopic neurons were also associated with increased propensity of EdU incorporation (Figures 4F and 4G), which supports a notion that vascular input contributes significantly to local cellular proliferation, metabolism, and neurogenesis. These results are fully in line with blood vessels being an essential constituent of the V-SVZ neurogenic niche. They suggest that increased vascular abundance in Fln[KO] brains not only facilitates the delivery of substrates for OXPHOS but also increases the flux of numerous extrinsic factors, such as growth factors, hormones, and endothelium-derived molecules, which are together necessary for NSPC self-renewal and neuronal differentiation.
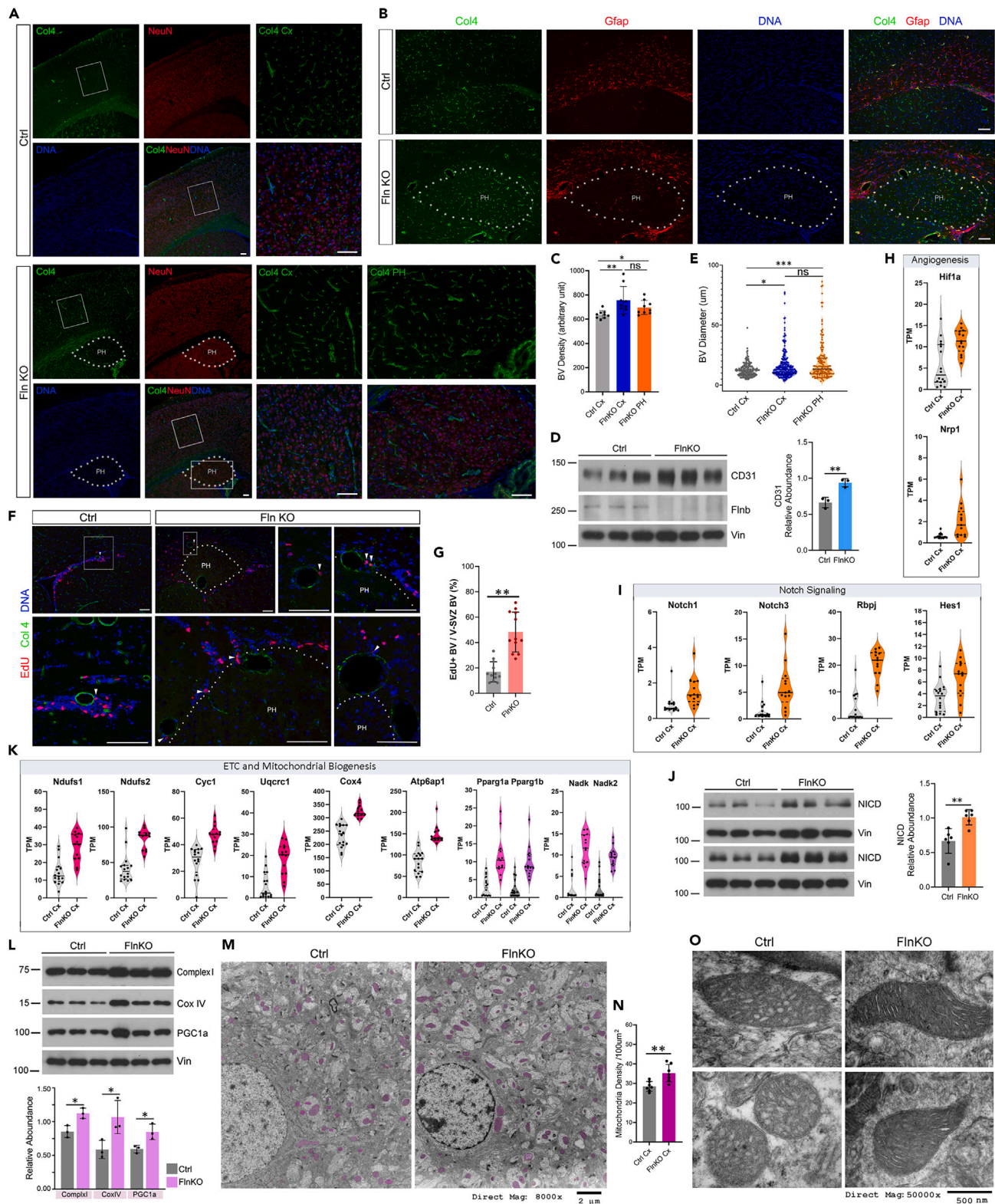
Figure 4. Increased vascularization and upregulation of energy metabolic activities throughout the neocortex of Fln^KO mice

(A) Representative images of Collagen IV (Col4, green) and NeuN (red) double immunostained brain sections of Fln^KO or control mice at weaning age. Nuclear DNA was stained with Hoechst 33342 and shown in blue. High-magnification images of boxed regions are included. The position of PH is marked by dotted lines.

Figure 4. Continued

(B) Representative images of Collagen IV (Col4, green) and Gfap (red) double immunostained brain sections of Fln^KO or control mice at 4 months of age. Nuclear DNA was stained with Hoechst 33342 and shown in blue. The positions of PH are marked by dotted lines.

(C) Quantification of blood vessel densities in the neocortex (Cx) of control or Fln^KO mice and in periventricular heterotopia (PH). Samples were from mice at 1–4 months of age ($n \geq 5$ each genotype). Shown are mean $\pm$ SD. *$p < 0.05$; **$p < 0.005$ by one-way ANOVA.

(D) CD31 immunoblotting analysis of cortical total protein extracts of Fln^KO and control mice at 4 months of age. Shown are representative images and mean $\pm$ SD; **$p < 0.005$ by Student's t test.

(E) Quantification of the caliber of blood vessels in neocortex (Cx) of control or Fln^KO mice and in periventricular heterotopia (PH). Samples were from mice at 1–4 months of age ($n \geq 5$ each genotype). Shown are violin plots with data points, median, and quartiles. *$p < 0.05$; ***$p < 0.001$ by Kolmogorov-Smirnov test.

(F) Representative images of brain sections of 3-month-old Fln^KO and control mice stained by EdU (red) and immunostained by anti-Col4 (green). Nuclear DNA was stained with Hoechst 33342 and shown in blue. High magnification images of boxed regions are included. The position of PH is marked by dotted lines. Arrowheads indicate EdU+ cells associated with enlarged blood vessels.

(G) Quantification of the correlation between EdU+ cells and blood vessels. Shown are % of blood vessels with juxtaposing EdU+ nuclei (arrows) in V-SVZs of Fln^KO and control mice ($n = 4$ biological replicates). Data points represent counts on each V-SVZ image with mean $\pm$ SD, **$p < 0.005$ by Student's t test.

(H) Expression levels (transcripts per million/TPM) of angiogenesis genes Hif1a and Nrp1 that were significantly upregulated across upper cortical layer ROIs of Fln^KO mice relative to those of control mice.

(I) Violin plots show that the expression level of selected genes in Notch signaling pathway were significantly upregulated across upper cortical layer ROIs of Fln^KO mice relative to those of control mice.

(J) Notch intracellular domain (NICD) immunoblotting analysis of cortical total protein extracts from Fln^KO and control mice at 4 months of age. Shown are representative images and mean $\pm$ SD; **$p < 0.005$ by Student's t test.

(K) Violin plots of selected genes mediating ETC function and mitochondrial biogenesis of which expression levels were significantly upregulated across upper cortical layer ROIs of Fln^KO mice relative to those of control mice.

(L) Immunoblotting analysis of total cortical protein extracts. Shown are representative IB images and quantifications (mean $\pm$ SD). *$p < 0.05$ by Student's t test.

(M) Representative electron micrographs of the neocortex of Fln^KO and control mice at 5 months of age. Mitochondria are highlighted in mauve.

(N) Quantification of mitochondrial density in the neocortex of Fln^KO and control mice at 5 months of age. Shown are mean $\pm$ SD. **$p < 0.005$ by Student's t test.

(O) Representative electron micrographs of mitochondria in the neocortex of Fln^KO and control mice at 5 months of age.

Scale bars: 100 μm or as indicated.

See also Figures S3 and S5.

Increased vascularization in the Fln^KO cortices was further supported by our GeoMx DSP data, which showed significant upregulation of several genes essential for angiogenesis in upper neocortical ROIs. Among transcripts significantly upregulated in the neocortex of Fln^KO mice, Hif1a is a potent transcriptional activator of angiogenesis; Nrp1 (Neuropilin 1) can also promote angiogenesis by acting as the receptor for Vegf and/or Sema3A (Figure 4H). In addition, several transcripts in the Notch signaling pathway were significantly upregulated in upper cortical ROIs of Fln^KO mice relative to those of control mice. These included the Notch1 and Notch3 receptors, the central Notch effector Rbpj, and the transcription target of Notch signaling Hes1 (Figure 4I). Notch signaling plays an essential role in angiogenesis by regulating endothelial tip cell formation, sprouting, and stabilization.[67] The activated Notch receptors are proteolytically cleaved and released as the Notch intracellular domain (NICD). We thus validated increased Notch signaling by determining the abundance of NICD and confirmed its significant elevation in Fln^KO relative to control cortices (Figure 4J). Although Notch signaling has been implicated in V-SVZ neurogenesis, upregulation of multiple Notch pathway genes, along with Hif1a and Nrp1, occurred specially in upper cortical ROIs of Fln^KO mice. This suggests that in Fln^KO mice, V-SVZ angiogenesis is driven primarily by EMT, whereas angiogenesis is regulated by Notch and Nrp1 signaling that spans over broad brain tissue.

The increase in cerebral vascular abundance is expected to have an impact at the systems level, affecting global brain metabolism and function. Consistent with this, genes mediating ETC function and mitochondrial biogenesis were also enriched in upper cortical ROIs of Fln^KO mice (Figure 4K). We further validated the transcriptional upregulation of oxidative ATP synthesis in Fln^KO cortices by immunoblotting (IB) and ultrastructure analyses. As expected, the cortical tissue of Fln^KO mice showed significantly increased abundance of proteins and structures for OXPHOS compared to that of control mice. These include the 75 kDa Ndufs1 subunit of respiratory complex I, the Cox 4 subunit of complex IV, the master regulator of mitochondria biogenesis PGC-1α, and the density of mitochondria (Figures 4L–4N). Similar to that observed in the V-SVZ, mitochondria in the neocortex of Fln^KO brains showed densely packed cristae (Figure 4O), suggesting robust ETC activities for ATP synthesis.

To further reveal the vascular impact on global brain metabolic activities, we examined the hippocampus of Fln^KO mice. Besides the V-SVZ, the dentate gyrus of hippocampus is the most active site of neurogenesis in adulthood across all mammals.[68–72] Although changes in hippocampal morphology and cellular composition were not evident, Fln^KO mice exhibited a significantly higher rate of EdU incorporation in the dentate gyrus relative to their control counterparts (Figure S5). This suggests that increases in cerebral vascular abundance had a brain system-wide influence on cell proliferative and metabolic activities in Fln^KO mice. Notably, the total number of EdU+ cells in dentate gyrus was much lower than that in V-SVZ of both Fln^KO and control mice, which could account for the lack of discernible differences in hippocampus structure.

Transcriptional co-upregulation of genes for brain metabolism, cell signaling, neurodevelopment, and neuronal activities in Fln^KO cortices

The global metabolic activation in Fln^KO brains was also demonstrated by differential transcriptome profiles identified across ROIs of upper cortical layers between Fln^KO and control mice. Out of the total 7,411 DEGs, the 4,609 upregulated genes in upper cortex of Fln^KO mice
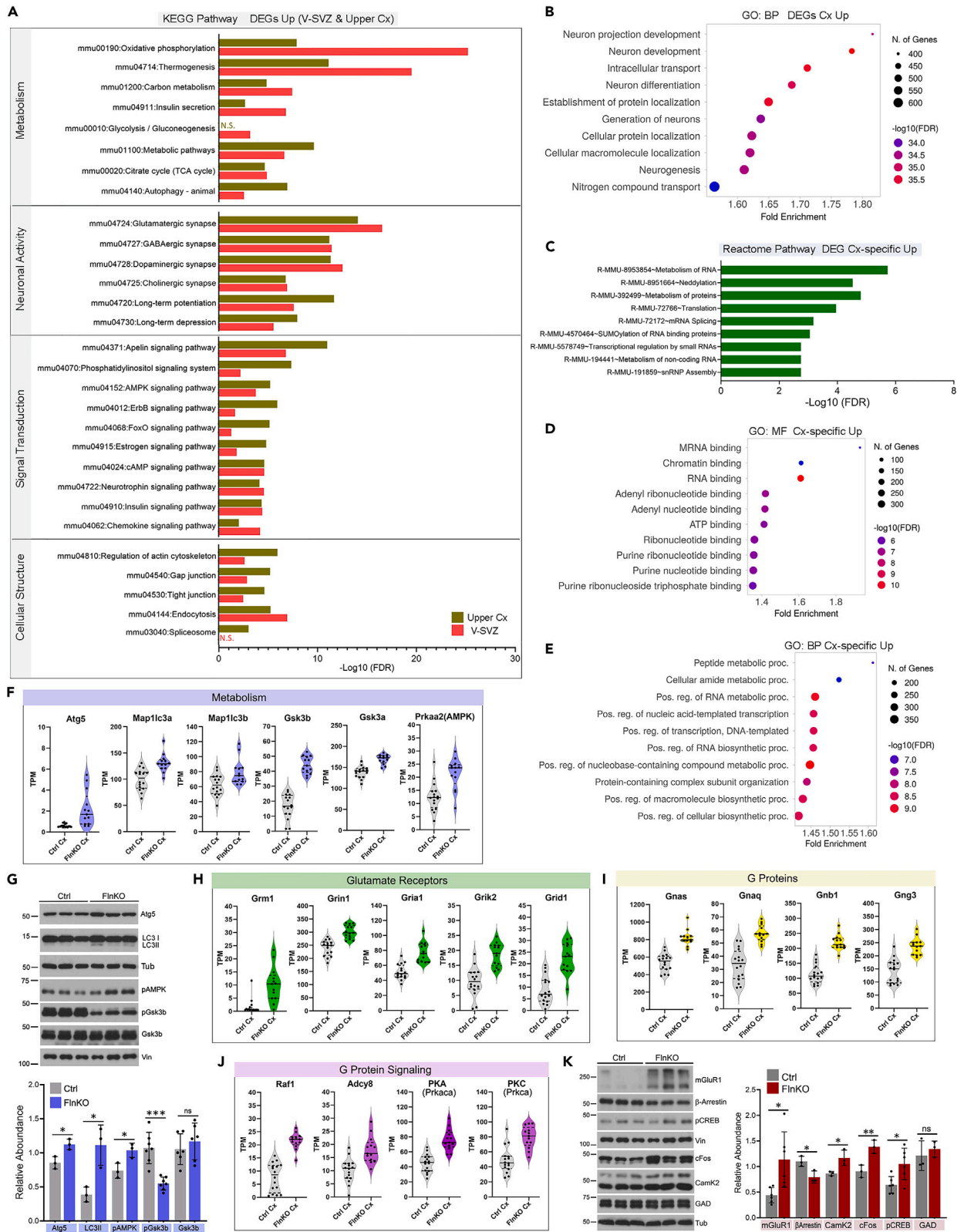
CellPress
OPEN ACCESS

Figure 5. Neocortical upregulation of genes mediating energy metabolism, cell signaling, and neuronal activities in Fln^KO mice

(A) KEGG pathway analysis of upregulated DEGs in V-SVZ or upper cortical layer ROIs of Fln^KO mice compared to those of control mice. Note the more significant upregulation of genes mediating OXPHOS and thermogenesis in V-SVZ ROIs than upper cortical ROIs and the more significant upregulation of genes essential for autophagy, LTP, LTD, Apelin signaling, and spliceosome in upper cortical ROIs than V-SVZ ROIs in Fln^KO mice.

(B) Gene Ontology biological processes (BP) terms enriched in all DEGs upregulated across upper cortical layer ROIs of Fln^KO mice compared to those of control mice.

(C) Reactome pathways overrepresented by DEGs exclusively upregulated across upper cortical layer ROIs of Fln^KO mice compared to those of control mice.

(D) Gene Ontology molecular function (MF) terms enriched in DEGs exclusively upregulated across upper cortical layer ROIs of Fln^KO mice compared to those of control mice.

(E) Gene Ontology biological processes (BP) terms enriched in DEGs exclusively upregulated across upper cortical layer ROIs of Fln^KO mice compared to those of control mice.

(F) Expression levels (transcripts per million/TPM) of selected genes mediating autophagy and metabolism that were significantly upregulated across upper cortical layer ROIs of Fln^KO mice relative to those of control mice.

(G) Immunoblotting analysis of total cortical protein extracts. Shown are representative IB images and quantifications (mean $\pm$ SD). ***$p < 0.001$; *$p < 0.05$ by Student's t test.

(H–J) Expression levels (transcripts per million/TPM) of selected glutamate receptors, G proteins, and molecules downstream of G protein signaling that were significantly upregulated across upper cortical layer ROIs of Fln^KO mice relative to those of control mice.

(K) Immunoblotting analysis of total cortical protein extracts. Shown are representative IB images and quantifications (mean $\pm$ SD). **$p < 0.005$; *$p < 0.05$ by Student's t test.

See also Figures S3, S6, and S7.

showed significant overrepresentation in numerous pathways not only for energy metabolism but also for neuronal activity, signal transduction, and cellular structure regulation (Figures 3A, 5A, and S3). Besides OXPHOS and the TCA cycle, upregulation in metabolic pathways extends to thermogenesis, carbon metabolism, and autophagy. In parallel, transcripts encoding molecules for glutamatergic, dopaminergic, GABAergic, and cholinergic synapses, as well as neuronal activity pathways in long-term potentiation (LTP) and long-term depression (LTD) were all enriched in upper cortical ROIs of Fln^KO than those of control mice. The transcriptomic elevation in brain metabolism and neuronal activity was also accompanied by increased expression of genes mediating diverse cell signaling cascades, including Apelin, phosphoinositide, AMPK, ErbB, FoxO, and cAMP pathways (Figures 5A and S6A–S6D). Many of these signaling pathways play important roles in regulating brain metabolism, neurodevelopment, neuronal excitability, and synaptic transmission. Their co-upregulation may support brain system-wide changes in Fln^KO mice.

As there is a substantial overlap in pathways overrepresented by upregulated DEGs in V-SVZ and upper cortical ROIs of Fln^KO mice, we determined their brain regional specificity. Although genes in pathways of OXPHOS, thermogenesis, insulin secretion, and gluconeogenesis were significantly upregulated in both V-SVZ and upper cortex of Fln^KO mice, their enrichments in V-SVZ were more pronounced than in upper cortical layers (Figure 5A), suggesting a stronger demand of upregulating aerobic glucose catabolism for V-SVZ neurogenesis. In contrast, genes mediating LTP, LTD, autophagy, and Apelin signaling were more significantly enriched in upper cortical than V-SVZ ROIs of Fln^KO mice (Figure 5A). LTP and LTD are important for synaptic communication and plasticity; autophagy is also crucial for neuronal-activity-mediated metabolic recycling that may facilitate neuronal connectivity and synaptic remodeling; the major role of Apelin signaling is promoting angiogenesis and vasodilation. Therefore, the co-upregulation of molecules in these pathways and increased vascular abundance in Fln^KO cortices can have a synergistic impact on the molecular turnover, synaptic signaling, and plasticity of neocortical neurons. In line with this, biological processes overrepresented by upper cortical ROIs in Fln^KO mice were predominantly related to nervous system development, including GO BP terms in neuron development, neuron differentiation, and intracellular transport (Figure 5B). Taken together, these data suggest that with vascular enrichment, V-SVZ's neurogenic activation in Fln^KO mice is coordinated with brain-wide boost of neuronal signaling and network activities.

To further validate the transcriptional elevation in activities and metabolic turnovers of Fln^KO cortical neurons, we queried the 2,874 DEGs that were exclusively upregulated in upper cortical ROIs (Figure S3E). We found these transcripts specifically enriched in upper cortical layers of Fln^KO mice overrepresented those Reactome pathways largely associated with RNA and protein metabolic synthesis, modification, and turnover (Figure 5C). Likewise, GO enrichment analyses showed that these upper-cortical-specific DEGs were significantly associated with MF and BP terms in RNA or nucleotide binding as well as RNA and peptide metabolic processes (Figures 5D and 5E). Such upregulation of genes for RNA and protein turnovers makes it possible for rapid molecular exchanges required for synaptic signaling and neuronal connectivity over a wide range. This is also in alignment with the activation of numerous essential molecules for brain metabolism in Fln^KO cortices at both mRNA and protein levels. Besides autophagy-associated genes, upper cortical ROIs of Fln^KO mice showed a remarkable upregulation in Gsk3b along with significant increases in Gsk3a and Prkaa2 encoding the catalytic subunit of AMPK (Figures 5F and S6E). Although Gsk3 can regulate a diverse array of cellular activities, it plays a primary role in glucose metabolism and energy homeostasis. The activation of Gsk3 is regulated by the removal of inhibitory phosphorylation, leading to diminished glucose storage and activated glycogen mobilization and glucose utilization. With increased Gsk3b, Gsk3a, and Prkaa2 mRNAs, Fln^KO cortical tissues also showed a significant reduction in the inhibitory phospho-Gsk3b and an elevation in the simulative phospho-AMPK (Figure 5G). AMPK is an important energy-sensing enzyme that activates energy production and inhibits energy consumption. Therefore, the coactivation of both GSK3 and AMPK is fully aligned with increased oxidative ATP synthesis in Fln^KO brains.

The adult brain is the top energy-consuming organ where ATP is mainly used to support synaptic transmission and neuronal communication. While upper cortical ROIs of Fln[KO] mice showed enriched transcripts for a wide range of synaptic activities (Figure 5A), glutamate synapses dominate excitatory activities for major cortical functions. Notably, 18 of the total 26 glutamate receptor genes were found significantly upregulated in upper cortical ROIs of Fln[KO] than those of controls (Figures 5H and S6F). These include glutamate metabotropic receptors as well as ionotropic receptors of NMDA, AMPA, kainite, and delta subtypes. Metabotropic glutamate receptors belong to G-protein-coupled receptors (GPCRs) that signal through G proteins; ionotropic glutamate receptors are ligand-gated ion channels that are also regulated by GPCRs and G protein signaling. We found that the transcriptional upregulation of glutamate receptors in upper cortical ROIs of Fln[KO] mice were coupled with significant enrichment of mRNAs encoding G proteins and key molecules of their downstream MAPK, cAMP, or phosphatidylinositol signaling pathways, including Raf1, adenylate cyclase Adcy8, Prkaca, and Prkca that encode PKA and PKC, respectively (Figures 5I and 5J). This suggests upper Fln[KO] cortices were poised to GPCR hyperstimulation and excitatory activities. Interestingly, we found β-Arestin, a molecule essential for attenuating GPCRs and downstream signaling, was decreased significantly at the protein level along with increases in glutamate signaling proteins, such as mGluR1, CamK2, c-Fos, and phospho-CREB (Figure 5K). In addition to diverse GPCRs,[49,73,74] FLNA also interacts with β-Arestin and plays a role in modulating cell signaling kinetics in embryonic cortices.[15] Therefore, a direct impact of Flna on β-Arestin stabilization, GPCR turnover, and downstream signaling remains plausible in the adult cortex. Collectively, our data suggest that increased V-SVZ neurogenesis and OXPHOS are associated with not only vascular enrichments but also increased excitatory activities in Fln[KO] cortices.

Consistent with the role of filamin in mediating numerous protein-protein interactions encompassing the actin cytoskeleton and diverse cytoplasmic or nuclear molecules, upregulated genes in both upper cortical and V-SVZ ROIs of Fln[KO] mice were associated with pathways regulating actin cytoskeleton, gap junction, tight junction, endocytosis, membrane trafficking, and protein-protein interactions at synapses (Figures 5A, S6A, and S6B). In addition, GO analysis showed that upregulated DEGs in Fln[KO] cortices were enriched in those CC terms essential for neurons, including synapses, dendrites, axons, myelin sheath, and mitochondrion, and those MP terms involving diverse molecular bindings of RNAs, proteins and protein complexes, protein kinases, transcriptional factors, chromatin, cytoskeleton, and nucleotides (Figures S7A and S7B). In contrast to the extensive functional annotation of upregulated genes, the 2,802 downregulated DEGs across upper cortical ROIs of Fln[KO] mice showed limited association with biological processes and functional pathways. Similar to the 1,489 downregulated genes in V-SVZ ROIs, genes downregulated in upper cortical layers of Fln[KO] mice were enriched most significantly in the BP term of "response to pheromone" (Figures S7C and S7D). These downregulated genes in Fln[KO] cortices were largely enriched in structures associated with extracellular matrix (ECM) and cell-cell or cell-ECM junctions where they mediate various binding activities for posttranslational modifications (Figures S7E and S7F). KEGG pathway analysis suggested that downregulated DEGs in upper cortical ROIs of Fln[KO] mice were weakly associated (-Log10 FDR = 1.5–1.7) with a few functional pathways such as cytokine receptor binding, hippo signaling, nuclear factor kB (NF-kB) signaling, regulation of stem cell pluripotency, necroptosis, and cancer (Figures S7G and S7H), which overall suggested altered restrictions in cell growth, survival, responses, and homeostasis. Altogether, with increased vascularization, OXPHOS, and metabolic turnovers of RNA and proteins, synaptic signaling, and neuronal activities, both V-SVZ and neocortex of adult Fln[KO] mice appear to be in a relatively immature and hyperactive state, retaining more features of a youthful, developing brain.

Periventricular neurons show transcriptome resemblance with upper cortical neurons but reduced expression of neuronal activity genes

We next determined the characteristics of neurons generated in the postnatal and adult V-SVZ by asking how neurons in PH nodules differ from those in upper cortical layers in Fln[KO] mice, since both regions are predominantly composed of Cux1^{+} neurons (Figure 1I). In contrast to the substantial transcriptomic difference in upper cortical layers between Fln[KO] and control mice, only 612 genes showed differential expression between PH and upper cortical ROIs of Fln[KO] mice (Figure 3A). This indicates that upper cortical neurons in Fln[KO] mice share a greater degree of molecular resemblance with periventricular neurons than with their upper cortical counterparts in control mice. Furthermore, the 612 DEGs showed no enrichment in genes representing olfactory neurons, which ruled out the possibility that periventricular neurons came from excessive generation or failed migration of olfactory neurons in Fln[KO] mice. Instead, the 167 DEGs upregulated in PH ROIs were moderately associated with tube morphogenesis, gliogenesis, ECM organization, and response to stimuli. The 445 DEGs downregulated in PH ROIs showed significant overrepresentation of pathways and biological processes in neurodevelopment and synaptic activities, including synaptic signaling, neuronal system, neuron projection development, regulation of membrane potential, organelle localization, membrane trafficking, behavior, as well as Ca^{2+} regulation and signaling by Rho GTPase (Figures 6A, 6B, and S8). In contrast to the remarkable transcriptional upregulation in cell signaling and neuronal communication in the upper cortex, multiple genes encoding synaptic signaling molecules were expressed at a significantly lower level in PH ROIs of Fln[KO] mice (Figure 6C). Notably, many transcripts for glutamate receptors, G proteins, and G protein signaling molecules were significantly downregulated in PH ROIs (Figures 6D–6F). In parallel to decreased gene expression in excitatory neuronal signaling, PH ROIs also showed transcriptional downregulation of ionotropic and metabotropic GABA receptors along with ion pumps and channels essential for membrane potential regulation, such as Na^{+}/K^{+} ATPase (Atp1a1 and Atp1b1), the inward K^{+} channel Kcnj3, and voltage-gated Na^{+} channel Scn1b (Figures 6G and 6H). This suggests that neurons in periventricular nodules were in an overall less active state compared to their upper cortical counterparts. Moreover, PH ROIs showed significantly decreased expression of genes mediating neuronal projection development (Figure 6I). Thus, the transcriptional downregulation in both synaptic signaling and neuronal morphogenesis of PH ROIs suggests that although the postnatal and adult V-SVZ of Fln[KO] mice retain the potential of generating neurons destined for the neocortex, neurons produced outside of the normal window of cortical development failed to become fully active as they were unable to
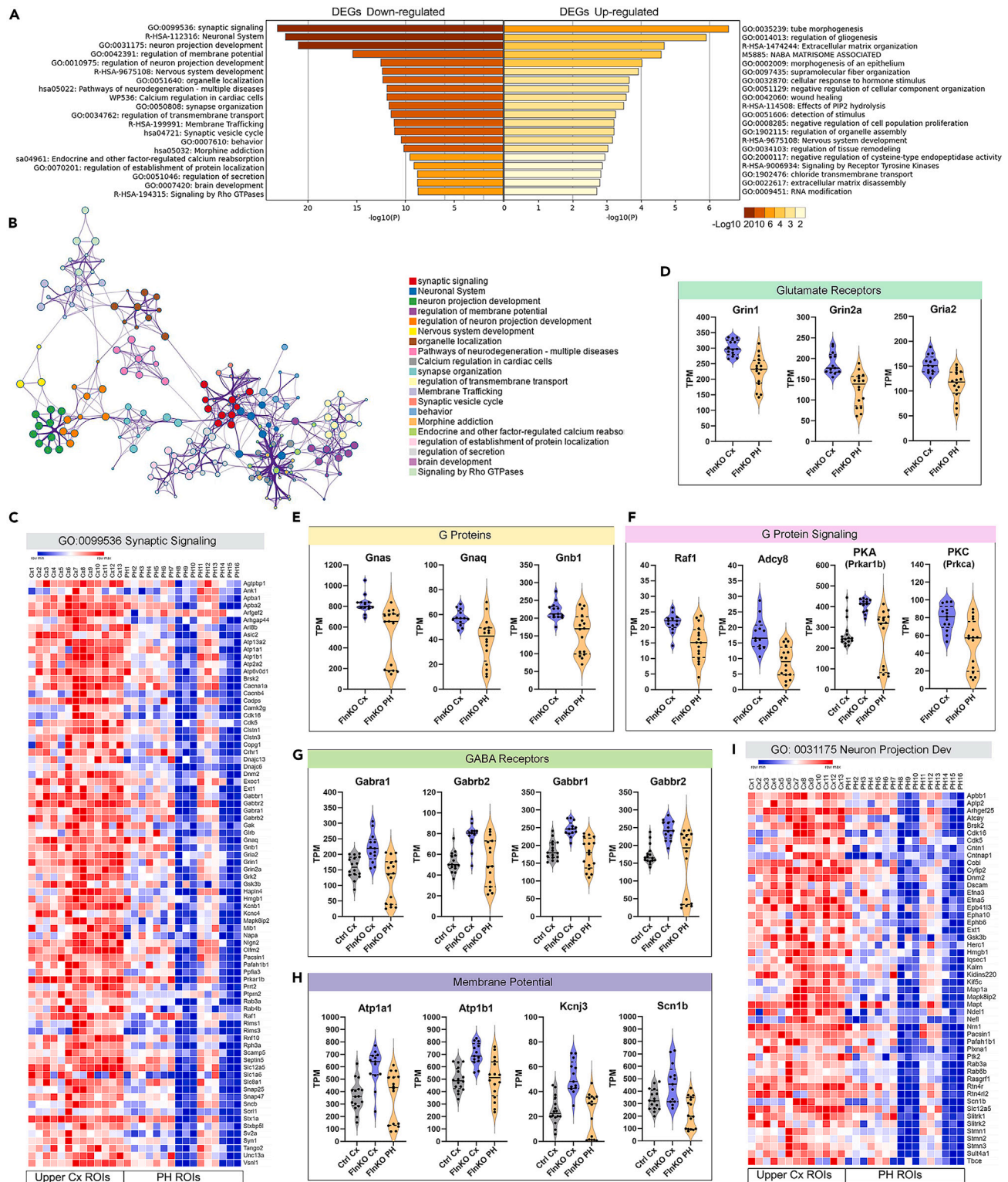
Figure 6. The transcriptome profiles of PH and upper cortical layers in Fln^KO mice differ mainly in synaptic signaling and neuronal morphogenesis

(A) Statistically enriched GO terms, KEGG or canonical pathways, and hallmark gene sets in DEG upregulated or downregulated between ROIs of periventricular nodules and ROIs of upper cortical layers of Fln^KO mice.

(B) Network of genes downregulated in ROIs across periventricular nodules compared to ROIs across upper cortical layers of Fln^KO mice.

Figure 6. Continued

(C) Heatmap representation of the expression levels of synaptic signaling genes that were significantly enriched in ROIs of upper cortical layers relatively to those of periventricular nodules of Fln[KO] mice.

(D–H) Violin plots show the expression levels of selected glutamate receptors, G proteins, molecules downstream of G protein signaling, GABA receptors, and molecules essential for membrane potential that were significantly downregulated in ROIs of periventricular nodules relative to those of upper cortical layer of Fln[KO] mice.

(I) Heatmap representation of the expression levels of neuron projection development genes that were significantly enriched in ROIs of upper cortical layers relatively to those of periventricular nodules of Fln[KO] mice.

See also Figure S8.

integrate into the functional cortical circuitry. Therefore, the major difference between neurons in periventricular nodules and upper cortical layers lies in the functional activity instead of neuronal subtype identity.

To validate that Fln[KO] neurons in periventricular nodules were less active than those in upper cortical layers, we first examined their levels of c-Fos protein that is commonly used as a marker for neuronal activity.[75] Despite an overall increase in cortical tissues of Fln[KO] than that of control mice (Figure 5K), c-Fos's immunoreactivity was predominantly presented by upper cortical neurons and was notably weaker or undetectable in neurons of the periventricular nodules in our IH analysis (Figures 7A and 7B). Similarly, the significant elevation of glutamate receptor mGluR1 (Grm1) in Fln[KO] cortices was largely exhibited by upper cortical neurons, though it was highly expressed in a small population of periventricular neurons (Figures 7C and 7D). We further showed that compromised c-Fos and mGluR1 in periventricular neurons were accompanied by reduced Camk2, the calcium-/calmodulin-dependent protein kinase that mediates excitatory glutamate signals underlying neuronal plasticity and learning. Although various Camk2 isoforms, including Camk2a, Camk2b, Camk2g, and Camk2n, were among DEGs upregulated in both V-SVZ and upper cortical ROIs of Fln[KO] compared to control mice (Figures 7E, S3B, S3C, S6C, and S6D), we found immuno-signals of CamK2 were considerably weaker in periventricular neurons than in upper cortical neurons of the same cortical section (Figure 7F). Such joint reduction in glutamate receptors, Camk2, and c-Fos in periventricular neurons fully corroborates our spatial transcriptomics data. They together indicate that neurons produced in the postnatal/adult V-SVZ of Fln[KO] mice were in a relatively dormant state compared to neocortical neurons generated during embryonic development.

Further supporting the relatively inactive state of periventricular neurons, we found there were fewer parvalbumin-expressing (PV+) GABAergic neurons in periventricular heterotopia nodules. PV+ inhibitory interneurons in the neocortex are derived from the ganglionic eminence in embryogenesis. In mice, these neurons migrate tangentially to the cortex, reach a steady state at the end of second postnatal week, adopt their electrophysiological properties at weaning age, and play important roles in regulating the activity of cortical glutamatergic excitatory neurons.[76,77] Correlated with the higher expression of GABA receptors in upper cortical than in PH ROIs, our IH analysis found the abundance of PV+ neurons was significantly elevated in the neocortex of Fln[KO] brains than that of control brains but was significantly reduced in periventricular nodules (Figures 6G and 7G). PV+ interneurons are important for excitation-inhibition balance, and their maturation and coupling to glutamatergic neurons contribute to the development of gamma oscillation and enhance cortical circuit performance.[78,79] Therefore, the enrichment of PV neurons and GABA receptors in the neocortex, coupled with their deficiency in PH, suggest that neural network activities in Fln[KO] brains are predominantly conducted by neurons in the neocortex, whereas the contribution of periventricular neurons born in postnatal/adult V-SVZ is likely minimal.

Despite a molecular function of filamin in cross-linking actin filaments, neither cortical nor periventricular neurons in Fln[KO] mice showed gross structural aberrations by Golgi-Cox stain and morphology analysis, though neurons in PH failed to develop proper spatial organization (Figures 7I and S9). Nonetheless, both heterotopic and cortical neurons in Fln[KO] mice showed significant increases in dendritic spine density compared to that of cortical neurons in control mice (Figure 7J). In addition, the spine morphology of filamin-deficient neurons was notably distorted. Although changes in spine head size and neck length were undetectable, Fln[KO] neurons showed thinner spine necks and a significant increase in perforated spines,[80,81] exhibiting doughnut-shaped, horseshoe-shaped, or claw-like glomerular endings (Figures 7K–7N). As these spine morphology features are largely shared between neocortical and periventricular neurons in Fln[KO] mice, it suggests that they could result directly from actin cytoskeleton defects due to filamin LOF. Nonetheless, the higher spine density, thinner spine neck, and increases in perforated spines can together provide a larger number and highly fluid contact sites for synaptic transmission, which is consistent with the overall underdeveloped and highly plastic state of Fln[KO] brains. The reduced cellular mechanical strength and enhanced cellular plasticity may underline the gained activity of both Fln[KO] NSPCs and neurons.

DISCUSSION

Although generation of new neurons in the adult brain holds a promise for replenishing neurons lost due to brain injury or degeneration, studies in the past decades have only shown the acquisition of a handful of molecular markers for active NSPCs and neuroblasts or the production of a small number of neurons transiently in the adult brain. Direct evidence for the long-term survival and physiological function of these adult-born neurons remains lacking. As a result of these limitations, whether new neurons can be generated in the adult human brain has been controversial.[12,14,82] The result of this study demonstrates that a large quantity of neurons resembling neurons of the neocortex can be generated by the postnatal and adult V-SVZ in Fln[KO] mice, providing direct evidence on the neurogenic capacity of adult V-SVZ. Given the close genetic and phenotypic resemblance between Fln[KO] mice and the corresponding human PH condition, our result serves as a proof of concept for further exploring the potential of inducing V-SVZ neurogenesis in the adult human brain.
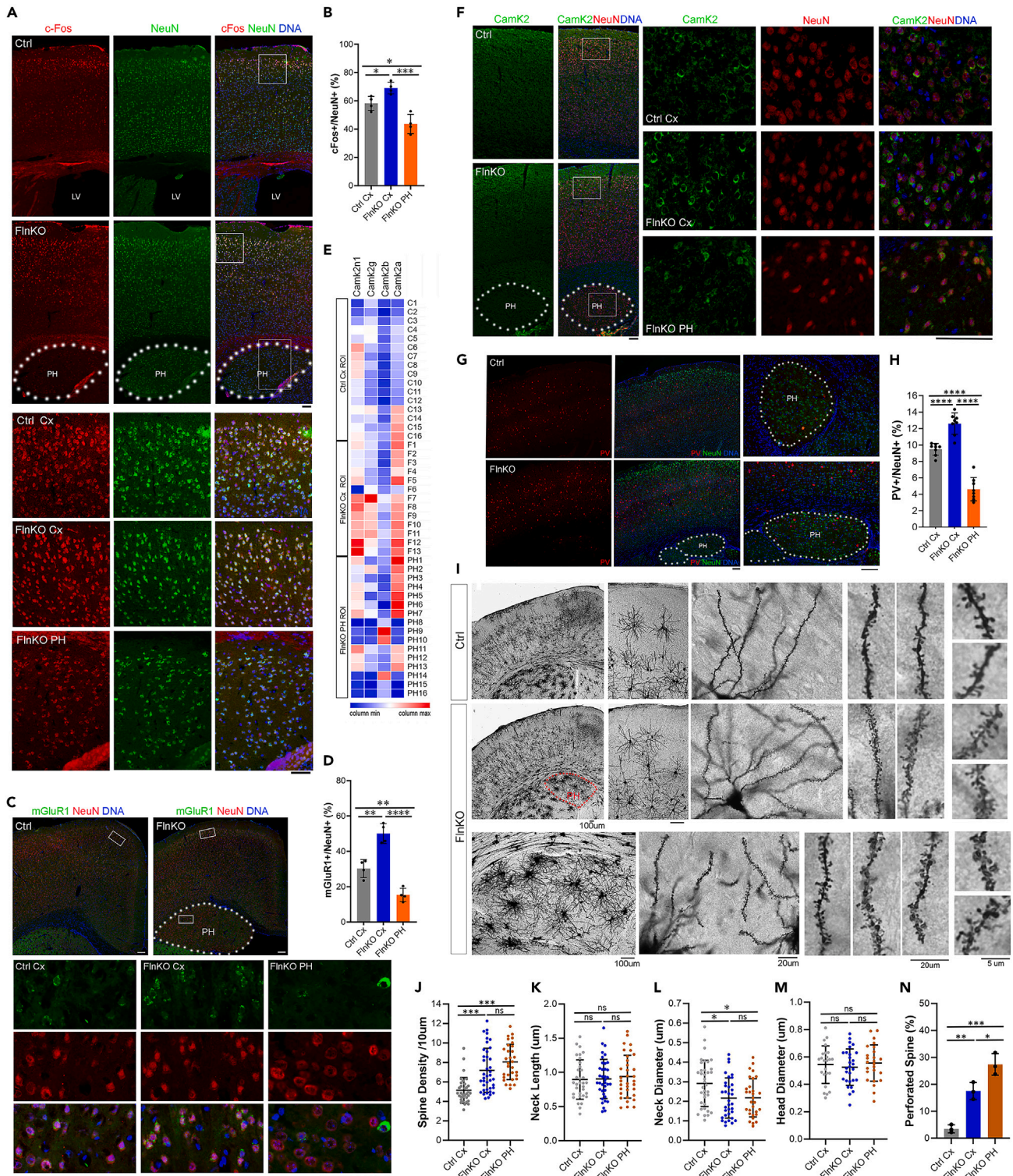
Figure 7. Neurons in periventricular nodules show compromised activity

(A) Representative images of cFos (red) and NeuN (green) double immunostained brain sections of Fln^KO or control mice at 3 months of age. Nuclear DNA was stained with Hoechst 33342 and shown in blue. High-magnification images of boxed regions are included. The position of PH is marked by dotted lines. Note the weak cFos immunosignals in periventricular neurons.

Figure 7. Continued

(B) Quantification of c-Fos+ neurons (% of total NeuN+) in upper cortical layers (Cx) of control or Fln^{KO} mice and periventricular heterotopia (PH) (n = 4 biological replicates). Shown are mean $\pm$ SD. *p < 0.05; ***p < 0.001 by one-way ANOVA.

(C) Representative images of mGluR1 (green) and NeuN (red) double immunostained brain sections of Fln^{KO} or control mice at 4 months of age. Nuclear DNA was stained with Hoechst 33342 and shown in blue. High-magnification images of boxed regions are included. The position of PH is marked by dotted lines. Note the strong mGluR1 immunosignals in a small fraction of periventricular neurons.

(D) Quantification of mGluR1+ neurons (% of total NeuN+) in upper cortical layers (Cx) of control or Fln^{KO} mice and periventricular heterotopia (n = 4 biological replicates). Shown are mean $\pm$ SD. **p < 0.005; ****p < 0.0001 by one-way ANOVA.

(E) Heatmap representation of the expression levels of several calcium-/calmodulin-dependent protein kinase type II (CamK2) genes in ROIs of upper cortical layers of control or Fln^{KO} mice and ROIs of periventricular nodules.

(F) Representative images of CamK2 (green) and NeuN (red) double immunostained brain sections of Fln^{KO} or control mice at 3 months of age. Nuclear DNA was stained with Hoechst 33342 and shown in blue. High-magnification images of boxed regions are included. The position of PH is marked by dotted lines. Note the weaker CamK2 immunosignals in periventricular neurons.

(G) Representative images of Parvalbumin (PV, red) and NeuN (green) double immunostained brain sections of Fln^{KO} or control mice at 4 months of age. Nuclear DNA was stained with Hoechst 33342 and shown in blue. The position of PH is marked by dotted lines.

(H) Quantification of PV + neurons (% of total NeuN+) in the neocortex (Cx) of control mice, the neocortex of Fln^{KO} mice, and periventricular heterotopia (PH). Shown are mean $\pm$ SD. ****p < 0.0001 by one-way ANOVA.

(I) Representative images of Golgi Cox-stained Fln^{KO} and control brains for neuronal morphology and dendritic spine analyses. Shown are images at various magnifications. Note that dendritic spines in Fln^{KO} mice show relatively thinner necks and doughnut or horseshoe shape with claw-like glomerular endings.

(J–M) Quantifications of dendritic spines' density, neck length, neck diameter, and head diameter in the neocortex (Cx) of control or Fln^{KO} mice and in periventricular heterotopia (PH) (n = 3 biological replicates). Shown are scatterplots with individual data points and mean $\pm$ SD, ***p < 0.001; *p < 0.05 by one-way ANOVA.

(N) The fractions (%) of doughnut- or horseshoe-shaped (perforated) spines in the neocortex (Cx) of control or Fln^{KO} mice and in periventricular heterotopia (PH) (n = 3 biological replicates). Shown are mean $\pm$ SD, ***p < 0.001; **p < 0.005; *p < 0.05 by one-way ANOVA.

Scale bars: 100 μm or as indicated.

See also Figure S9.

Despite extensive studies of neurogenesis in the brain, mechanisms underlying the intrinsic and extrinsic control of NSPCs' neurogenic propensity remain largely elusive. Nonetheless, at the systems level, it is conceivable that both intrinsic and extrinsic factors driving neuronal differentiation are well synchronized with the developmental state and physiological activities of the brain. This notion is well supported by results of this study. First, our data suggest that NSPCs' neurogenic propensity is highly regulated by the brain's energy metabolic status. In fetal development, brain metabolism is predominately mediated by anaerobic glycolysis.[83] After birth, the brain starts to receive oxygen-rich blood and gradually switches to aerobic catabolism of glucose. By adult age, brain energetics fully relies on OXPHOS, consuming 25% of glucose intake and 20% of inhaled oxygen in order to maintain neuronal communication and synaptic activities. To meet such energy demand of the adult brain, upregulation of genes participating OXPHOS must be necessary for activating the neuronal differentiation of NSPCs as we observed in the V-SVZ of adult Fln^{KO} mice. In close agreement, previous reports also demonstrated that the transition of neural stem cells to progenitor cells of the neuronal lineage was accompanied by increased mitochondrial biogenesis.[84,85] Moreover, our data indicate that generation of periventricular neurons in the V-SVZ of Fln^{KO} mice is correlated with increased expression of a myriad of genes involving synaptic transmission, neuronal plasticity, and metabolic turnovers in the neocortex. These data imply that in addition to ATP synthesis, neurogenic propensity of NSPCs in the postnatal and adult V-SVZ is well coordinated with neocortical neurons' state of differentiation, maturity, and physiological activity. Besides long-distance axonal communications, vitalized V-SVZ and upper cortical layers in Fln^{KO} mice may be functionally connected by vascular circulation. In this case, increased vascular abundance not only boosts oxidative metabolism and ATP synthesis within V-SVZ but also enhances brain-wide metabolic activation and function. Therefore, cerebral blood vessels are both an essential neurogenic niche and a prerequisite for neuronal function in the adult brain.

While the vascular enrichment acts as the external cue to enhance the energetics and activities of cortical NSPCs and neurons, filamin LOF is the intrinsic factor that renders NSPCs and neurons to an underdifferentiated immature state with high susceptibility and sensitized responses to external cues. This is consistent with our earlier finding that filamin LOF led to hyperactive Igf and Vegf signaling in the embryonic V-SVZ.[15] Such deficiency suggests that filamin acts as a gatekeeper for cell signaling and tissue homeostasis. Although filamin has been regarded as an actin stabilizer, the pleotropic phenotype of filamin LOF in humans and mice are not simply explained by deficiencies in actin crosslinking. Besides actin, filamin interacts with numerous molecules for cell sensing, signaling, gene expression, and morphogenesis. This allows it to coordinate intricate cell-cell interactions, signaling networks, intracellular structures, and metabolic processes in various tissue environments. Such unique characteristic of filamin is essential for maintaining the homeostasis and stability of cells bombarded by diverse extracellular cues. In line with this, *FLNA* mutations have been shown to affect the cardiovascular, skeletal, lungs, gastro, and connective tissues.[23,25,56,86,87] Recent studies also suggest a dual function of FLNa in cancer promotion and tumor suppression.[88] These are all fully in line with data presented in this study, which demonstrate that filamin LOF results in the reprograming of a wide range of molecular networks for cell signaling, cell mechanics, cell metabolism, and gene expression. These changes may decrease the homeostatic stability, resulting in sensitization and activation of NSPCs, glia, and neurons at a brain systems level.

Although epilepsy is the main neurological symptom of *FLNA* mutations, the condition can be asymptomatic and go silently without being detected by MRI. We have not observed spontaneous seizures in Fln^{KO} mice. However, our spatial transcriptomics data revealed a remarkable upregulation of genes mediating excitatory activities in upper layers compared to periventricular nodules. This suggests that seizure activities

in the human PH condition originate, at least in part, from hyperexcitabilities of neocortical neurons with *FLNA* deficiency. In general, seizure activities often result from shifts in inhibitory and excitatory imbalance toward excessive excitability. In Fln^{KO} mice, the density of inhibitory PV$^+$ neurons was significantly higher in the cortex but significantly lower in PH. It remains possible that a deficiency in GABAergic neurons in peri-ventricular nodules accounts for the hyperexcitability of seizure induction. However, reduced c-Fos, Camk2, and glutamate receptors in peri-ventricular neurons, along with a significant transcriptional downregulation in synaptic signaling, altogether suggest that heterotopic neurons are unfavorable candidates for hyperexcitability. Given that the survival, maturation, and activity of PV$^+$ neurons are influenced considerably by the activity of excitatory circuits, a more plausible interpretation is that the increase in PV$^+$ neurons in the neocortex of Fln^{KO} mice reflects a compensatory response to excitation-inhibition imbalance due to hyperactive glutamate signaling, whereas the low PV$^+$ neurons in the peri-ventricular nodules may be a sign of function immaturity of excitatory neurons generated by the postnatal and adult V-SVZ.

To date, our understanding of the neurogenic potential and functional significance of the adult V-SVZ is still at a very early stage. There is a pressing need for developing representative *in vivo* models to uncover the mechanisms for regulating cellular activities in the adult V-SVZ. Despite that heterotopic neurons generated in the juvenile and adult V-SVZ of Fln^{KO} mice appear unable to integrate into the cortical circuit and acquire full activity and function, these neurons closely resemble excitatory neurons in upper cortical layers. Therefore, this mouse model of human condition raises a possibility of inducing V-SVZ neurogenesis by targeting NSPC-vascular interaction and brain energy metabolism regulated by FLNA.

Limitations of the study

Although this study provides a direct evidence that the postnatal and adult V-SVZ retains the ability of generating neurons that resemble those in the neocortex with respect to transcriptome profiles, it remains challenging to fully define the underlying mechanism of NSPC activation in the adult V-SVZ. Our results suggest adult V-SVZ neurogenesis involves coordinated changes in a large number of molecules, cell types, and pathways at the brain systems level. Likewise, the function of filamin is also multifaceted and complex, which makes it difficult to delineate the precise molecular mechanism underlying functional alterations in V-SVZ and neocortex of Fln^{KO} mice. Our previous developmental study showed that filamin-deficient radial glial cells underwent sustained EMT, altering the microenvironment of neuronal-fate-restricted progenitors in the embryonic V-SVZ. Although Snail1, the prominent EMT inducer, remains highly upregulated in the V-SVZ of adult Fln^{KO} mice, additional work is required to define the molecular network downstream of Snail1's action. Given the numerous molecular interactions of filamin and the remarkable transcriptomic changes caused by filamin LOF, future studies are needed to determine the common and differential mechanisms of filamin in NSPCs of the embryonic and adult V-SVZ, neurons of the neocortex, and the neuro-vascular interface that synchronizes neural activities with vascular circulation.

STAR★METHODS

Detailed methods are provided in the online version of this paper and include the following:

- KEY RESOURCES TABLE
- RESOURCE AVAILABILITY
  - Lead contact
  - Materials availability
  - Data and code availability
- EXPERIMENTAL MODEL AND STUDY PARTICIPANT DETAILS
  - Mice
- METHOD DETAILS
  - Fluorescence immunohistological and immunochemical analyses
  - GeoMx Digital Spatial Profiling of the mouse whole-transcriptome
  - Ultra-structural analysis
  - Golgi-Cox staining for neuronal morphology and dendritic spine analysis
  - Immunoblotting
- QUANTIFICATION AND STATISTICAL ANALYSIS

SUPPLEMENTAL INFORMATION

Supplemental information can be found online at https://doi.org/10.1016/j.isci.2024.110199.

ACKNOWLEDGMENTS

![CellPress logo] OPEN ACCESS

AUTHOR CONTRIBUTIONS

DECLARATION OF INTERESTS

REFERENCES

1. Gotz, M., and Huttner, W.B. (2005). The cell biology of neurogenesis. Nat. Rev. Mol. Cell Biol. 6, 777–788. https://doi.org/10.1038/nrm1739.

2. Rakic, P. (1972). Mode of cell migration to the superficial layers of fetal monkey neocortex. J. Comp. Neurol. 145, 61–83. https://doi.org/10.1002/cne.901450105.

3. Noctor, S.C., Martínez-Cerdeño, V., Ivic, L., and Kriegstein, A.R. (2004). Cortical neurons arise in symmetric and asymmetric division zones and migrate through specific phases. Nat. Neurosci. 7, 136–144.

4. Taverna, E., Götz, M., and Huttner, W.B. (2014). The cell biology of neurogenesis: toward an understanding of the development and evolution of the neocortex. Annu. Rev. Cell Dev. Biol. 30, 465–502. https://doi.org/10.1146/annurev-cellbio-101011-155801.

5. Alves, J.A.J., Barone, P., Engelender, S., Fróes, M.M., and Menezes, J.R.L. (2002). Initial stages of radial glia astrocytic transformation in the early postnatal anterior subventricular zone. J. Neurobiol. 52, 251–265. https://doi.org/10.1002/neu.10087.

6. Toma, K., and Hanashima, C. (2015). Switching modes in corticogenesis: mechanisms of neuronal subtype transitions and integration in the cerebral cortex. Front. Neurosci. 9, 274. https://doi.org/10.3389/fnins.2015.00274.

7. Qian, X., Shen, Q., Goderie, S.K., He, W., Capela, A., Davis, A.A., and Temple, S. (2000). Timing of CNS cell generation: a programmed sequence of neuron and glial cell production from isolated murine cortical stem cells. Neuron 28, 69–80. https://doi.org/10.1016/s0896-6273(00)00086-6.

8. Kriegstein, A., and Alvarez-Buylla, A. (2009). The glial nature of embryonic and adult neural stem cells. Annu. Rev. Neurosci. 32, 149–184. https://doi.org/10.1146/annurev.neuro.051508.135600.

9. Sanai, N., Tramontin, A.D., Quiñones-Hinojosa, A., Barbaro, N.M., Gupta, N., Kunwar, S., Lawton, M.T., McDermott, M.W., Parsa, A.T., Manuel-García Verdugo, J., et al. (2004). Unique astrocyte ribbon in adult human brain contains neural stem cells but lacks chain migration. Nature 427, 740–744. https://doi.org/10.1038/nature02301.

10. Mizrak, D., Levitin, H.M., Delgado, A.C., Crotet, V., Yuan, J., Chaker, Z., Silva-Vargas, V., Sims, P.A., and Doetsch, F. (2019). Single-Cell Analysis of Regional Differences in Adult V-SVZ Neural Stem Cell Lineages. Cell Rep. 26, 394–406.e5. https://doi.org/10.1016/j.celrep.2018.12.044.

11. Alvarez-Buylla, A., and Garcia-Verdugo, J.M. (2002). Neurogenesis in adult subventricular zone. J. Neurosci. 22, 629–634. https://doi.org/10.1523/JNEUROSCI.22-03-00629.2002.

12. Nano, P.R., and Bhaduri, A. (2022). Mounting evidence suggests human adult neurogenesis is unlikely. Neuron 110, 353–355. https://doi.org/10.1016/j.neuron.2022.01.004.

13. Lim, D.A., and Alvarez-Buylla, A. (2016). The Adult Ventricular-Subventricular Zone (V-SVZ) and Olfactory Bulb (OB) Neurogenesis. Cold Spring Harbor Perspect. Biol. 8, a018820. https://doi.org/10.1101/cshperspect.a018820.

14. Duque, A., Arellano, J.I., and Rakic, P. (2022). An assessment of the existence of adult neurogenesis in humans and value of its rodent models for neuropsychiatric diseases. Mol. Psychiatr. 27, 377–382. https://doi.org/10.1038/s41380-021-01314-8.

15. Houlihan, S.L., Lanctot, A.A., Guo, Y., and Feng, Y. (2016). Upregulation of neurovascular communication through filamin abrogation promotes ectopic periventricular neurogenesis. Elife 5, e17823. https://doi.org/10.7554/eLife.17823.

16. Barkovich, A.J., and Kjos, B.O. (1992). Gray matter heterotopias: MR characteristics and correlation with developmental and neurologic manifestations. Radiology 182, 493–499.

17. Barkovich, A.J., and Kuzniecky, R.I. (2000). Gray matter heterotopia. Neurology 55, 1603–1608.

18. Eksioglu, Y.Z., Scheffer, I.E., Cardenas, P., Knoll, J., DiMario, F., Ramsby, G., Berg, M., Kamuro, K., Berkovic, S.F., Duyk, G.M., et al. (1996). Periventricular heterotopia: an X-linked dominant epilepsy locus causing aberrant cerebral cortical development. Neuron 16, 77–87.

19. Fox, J.W., Lamperti, E.D., Ekşioğlu, Y.Z., Hong, S.E., Feng, Y., Graham, D.A., Scheffer, I.E., Dobyns, W.B., Hirsch, B.A., Radtke, R.A., et al. (1998). Mutations in filamin 1 prevent migration of cerebral cortical neurons in human periventricular heterotopia. Neuron 21, 1315–1325.

20. Parrini, E., Ramazzotti, A., Dobyns, W.B., Mei, D., Moro, F., Veggiotti, P., Marini, C., Brilstra, E.H., Dalla Bernardina, B., Goodwin, L., et al. (2006). Periventricular heterotopia: phenotypic heterogeneity and correlation with Filamin A mutations. Brain 129, 1892–1906. https://doi.org/10.1093/brain/awl125.

21. Sheen, V.L., Dixon, P.H., Fox, J.W., Hong, S.E., Kinton, L., Sisodiya, S.M., Duncan, J.S., Dubeau, F., Scheffer, I.E., Schachter, S.C., et al. (2001). Mutations in the X-linked filamin 1 gene cause periventricular nodular heterotopia in males as well as in females. Hum. Mol. Genet. 10, 1775–1783.

22. Lange, M., Kasper, B., Bohring, A., Rutsch, F., Kluger, G., Hoffjan, S., Spranger, S., Behnecke, A., Ferbert, A., Hahn, A., et al. (2015). 47 patients with FLNA associated periventricular nodular heterotopia. Orphanet J. Rare Dis. 10, 134. https://doi.org/10.1186/s13023-015-0331-9.

23. Chen, M.H., and Walsh, C.A. (1993). FLNA Deficiency. In GeneReviews((R)), M.P. Adam, G.M. Mirzaa, R.A. Pagon, S.E. Wallace, L.J.H. Bean, K.W. Gripp, and A. Amemiya, eds.

24. Bernstein, J.A., Bernstein, D., Hehr, U., and Hudgins, L. (2011). Familial cardiac valvulopathy due to filamin A mutation. Am. J. Med. Genet. 155A, 2236–2241. https://doi.org/10.1002/ajmg.a.34132.

25. Reinstein, E., Frentz, S., Morgan, T., García-Miñaúr, S., Leventer, R.J., McGillivray, G., Pariani, M., van der Steen, A., Pope, M., Holder-Espinasse, M., et al. (2013). Vascular and connective tissue anomalies associated with X-linked periventricular heterotopia due to mutations in Filamin A. Eur. J. Hum. Genet. 21, 494–502. https://doi.org/10.1038/ejhg.2012.209.

26. Huttenlocher, P.R., Taravath, S., and Mojtahedi, S. (1994). Periventricular heterotopia and epilepsy. Neurology 44, 51–55.

27. d'Orsi, G., Tinuper, P., Bisulli, F., Zaniboni, A., Bernardi, B., Rubboli, G., Riva, R., Michelucci, R., Volpi, L., Tassinari, C.A., and Baruzzi, A. (2004). Clinical features and long term outcome of epilepsy in periventricular nodular heterotopia. Simple compared with plus forms. J. Neurol. Neurosurg. Psychiatry 75, 873–878. https://doi.org/10.1136/jnnp.2003.024315.

28. Battaglia, G., Chiapparini, L., Franceschetti, S., Freri, E., Tassi, L., Bassanini, S., Villani, F., Spreafico, R., D'Incerti, L., and Granata, T. (2006). Periventricular nodular heterotopia: classification, epileptic history, and genesis of epileptic discharges. Epilepsia 47, 86–97. https://doi.org/10.1111/j.1528-1167.2006.00374.x.

29. Reinstein, E., Chang, B.S., Robertson, S.P., Rimoin, D.L., and Katzir, T. (2012). Filamin A

mutation associated with normal reading skills and dyslexia in a family with periventricular heterotopia. Am. J. Med. Genet. *158A*, 1897–1901. https://doi.org/10.1002/ajmg.a.35455.

30. Chang, B.S., Ly, J., Appignani, B., Bodell, A., Apse, K.A., Ravenscroft, R.S., Sheen, V.L., Doherty, M.J., Hackney, D.B., O'Connor, M., et al. (2005). Reading impairment in the neuronal migration disorder of periventricular nodular heterotopia. Neurology *64*, 799–803. https://doi.org/10.1212/01.WNL.0000152874.57180.AF.

31. Felker, M.V., Walker, L.M., Sokol, D.K., Edwards-Brown, M., and Chang, B.S. (2011). Early cognitive and behavioral problems in children with nodular heterotopia. Epilepsy Behav. *22*, 523–526. https://doi.org/10.1016/j.yebeh.2011.08.010.

32. Lv, B., Zhou, Y., Zeng, J., Wang, L., Zhao, F., Chen, H., Li, X., Song, Y., Xiao, M., Ding, Z., and Cheng, B. (2022). Cases report: MRI findings of asymptomatically familial subependymal heterotopia with filamin A gene abnormality. Front. Neurosci. *16*, 956545. https://doi.org/10.3389/fnins.2022.956545.

33. Eisenbiegler, G.E., and Brown, S.A. (2021). Three Generations of FLNA-Associated Periventricular Nodular Heterotopia. Case Rep. Neurol. *13*, 777–781. https://doi.org/10.1159/000519507.

34. Guerrini, R., Mei, D., Sisodiya, S., Sicca, F., Harding, B., Takahashi, Y., Dorn, T., Yoshida, A., Campistol, J., Krämer, G., et al. (2004). Germline and mosaic mutations of FLN1 in men with periventricular heterotopia. Neurology *63*, 51–56.

35. Poussaint, T.Y., Fox, J.W., Dobyns, W.B., Radtke, R., Scheffer, I.E., Berkovic, S.F., Barnes, P.D., Huttenlocher, P.R., and Walsh, C.A. (2000). Periventricular nodular heterotopia in patients with filamin-1 gene mutations: neuroimaging findings. Pediatr. Radiol. *30*, 748–755.

36. Parrini, E., Rivas, I.L., Toral, J.F., Pucatti, D., Giglio, S., Mei, D., and Guerrini, R. (2011). In-frame deletion in FLNA causing familial periventricular heterotopia with skeletal dysplasia in males. Am. J. Med. Genet. *155A*, 1140–1146. https://doi.org/10.1002/ajmg.a.33880.

37. Ferland, R.J., and Guerrini, R. (2009). Nodular heterotopia is built upon layers. Neurology *73*, 742–743. https://doi.org/10.1212/WNL.0b013e3181b529b1.

38. Deleo, F., Hong, S.J., Fadaie, F., Caldairou, B., Krystal, S., Bernasconi, N., and Bernasconi, A. (2020). Whole-brain multimodal MRI phenotyping of periventricular nodular heterotopia. Neurology *95*, e2418–e2426. https://doi.org/10.1212/WNL.0000000000010648.

39. Wang, K., and Singer, S.J. (1977). Interaction of filamin with f-actin in solution. Proc. Natl. Acad. Sci. USA *74*, 2021–2025.

40. Weihing, R.R. (1985). The filamins: properties and functions. Can. J. Biochem. Cell Biol. *63*, 397–413.

41. Nakamura, F., Stossel, T.P., and Hartwig, J.H. (2011). The filamins: organizers of cell structure and function. Cell Adhes. Migrat. *5*, 160–169. https://doi.org/10.4161/cam.5.2.14401.

42. Gorlin, J.B., Yamin, R., Egan, S., Stewart, M., Stossel, T.P., Kwiatkowski, D.J., and Hartwig, J.H. (1990). Human endothelial actin-binding protein (ABP-280, nonmuscle filamin): a molecular leaf spring. J. Cell Biol. *111*, 1089–1105.

43. Weihing, R.R. (1988). Actin-binding and dimerization domains of HeLa cell filamin. Biochemistry *27*, 1865–1869.

44. Sheen, V.L., Feng, Y., Graham, D., Takafuta, T., Shapiro, S.S., and Walsh, C.A. (2002). Filamin A and Filamin B are co-expressed within neurons during periods of neuronal migration and can physically interact. Hum. Mol. Genet. *11*, 2845–2854.

45. Stossel, T.P., Condeelis, J., Cooley, L., Hartwig, J.H., Noegel, A., Schleicher, M., and Shapiro, S.S. (2001). Filamins as integrators of cell mechanics and signalling. Nat. Rev. Mol. Cell Biol. *2*, 138–145.

46. Lamsoul, I., Dupré, L., and Lutz, P.G. (2020). Molecular Tuning of Filamin A Activities in the Context of Adhesion and Migration. Front. Cell Dev. Biol. *8*, 591323. https://doi.org/10.3389/fcell.2020.591323.

47. Feng, Y., and Walsh, C.A. (2004). The many faces of filamin: a versatile molecular scaffold for cell motility and signalling. Nat. Cell Biol. *6*, 1034–1038.

48. Modarres, H.P., and Mofradt, M.R.K. (2014). Filamin: a structural and functional biomolecule with important roles in cell biology, signaling and mechanics. Mol. Cell. BioMech. *11*, 39–65.

49. van der Flier, A., and Sonnenberg, A. (2001). Structural and functional aspects of filamins. Biochim. Biophys. Acta *1538*, 99–117. https://doi.org/10.1016/s0167-4889(01)00072-6.

50. Kasper, B.S., Kurzbuch, K., Chang, B.S., Pauli, E., Hamer, H.M., Winkler, J., and Hehr, U. (2013). Paternal inheritance of classic X-linked bilateral periventricular nodular heterotopia. Am. J. Med. Genet. *161A*, 1323–1328. https://doi.org/10.1002/ajmg.a.35917.

51. Cannaerts, E., Shukla, A., Hasanhodzic, M., Alaerts, M., Schepers, D., Van Laer, L., Girisha, K.M., Hojsak, I., Loeys, B., and Verstraeten, A. (2018). FLNA mutations in surviving males presenting with connective tissue findings: two new case reports and review of the literature. BMC Med. Genet. *19*, 140. https://doi.org/10.1186/s12881-018-0655-0.

52. Walsh, M., Hebbard, G., and Trainer, A. (2017). Update on a previously reported male with a FLNA missense mutation. Eur. J. Hum. Genet. *25*, 905–906. https://doi.org/10.1038/ejhg.2016.156.

53. Oegema, R., Hulst, J.M., Theuns-Valks, S.D.M., van Unen, L.M.A., Schot, R., Mancini, G.M.S., Schipper, M.E.I., de Wit, M.C.Y., Sibbles, B.J., de Coo, I.F.M., et al. (2013). Novel no-stop FLNA mutation causes multi-organ involvement in males. Am. J. Med. Genet. *161A*, 2376–2384. https://doi.org/10.1002/ajmg.a.36109.

54. Bandaru, S., Ala, C., Zhou, A.X., and Akyürek, L.M. (2021). Filamin A Regulates Cardiovascular Remodeling. Int. J. Mol. Sci. *22*, 6555. https://doi.org/10.3390/ijms22126555.

55. Feng, Y., Chen, M.H., Moskowitz, I.P., Mendonza, A.M., Vidali, L., Nakamura, F., Kwiatkowski, D.J., and Walsh, C.A. (2006). Filamin A (FLNA) is required for cell-cell contact in vascular development and cardiac morphogenesis. Proc. Natl. Acad. Sci. USA *103*, 19836–19841.

56. Kyndt, F., Gueffet, J.P., Probst, V., Jaafar, P., Legendre, A., Le Bouffant, F., Toquet, C., Roy, E., McGregor, L., Lynch, S.A., et al. (2007). Mutations in the gene encoding filamin A as a cause for familial cardiac valvular dystrophy.

Circulation *115*, 40–49. https://doi.org/10.1161/CIRCULATIONAHA.106.622621.

57. Shen, Q., Wang, Y., Kokovay, E., Lin, G., Chuang, S.M., Goderie, S.K., Roysam, B., and Temple, S. (2008). Adult SVZ stem cells lie in a vascular niche: a quantitative analysis of niche cell-cell interactions. Cell Stem Cell *3*, 289–300. https://doi.org/10.1016/j.stem.2008.07.026.

58. Quaresima, S., Istiaq, A., Jono, H., Cacci, E., Ohta, K., and Lupo, G. (2022). Assessing the Role of Ependymal and Vascular Cells as Sources of Extracellular Cues Regulating the Mouse Ventricular-Subventricular Zone Neurogenic Niche. Front. Cell Dev. Biol. *10*, 845567. https://doi.org/10.3389/fcell.2022.845567.

59. Shen, Q., Goderie, S.K., Jin, L., Karanth, N., Sun, Y., Abramova, N., Vincent, P., Pumiglia, K., and Temple, S. (2004). Endothelial cells stimulate self-renewal and expand neurogenesis of neural stem cells. Science *304*, 1338–1340. https://doi.org/10.1126/science.1095505.

60. Jin, K., Zhu, Y., Sun, Y., Mao, X.O., Xie, L., and Greenberg, D.A. (2002). Vascular endothelial growth factor (VEGF) stimulates neurogenesis *in vitro* and *in vivo*. Proc. Natl. Acad. Sci. USA *99*, 11946–11950. https://doi.org/10.1073/pnas.182296499.

61. Licht, T., Rothe, G., Kreisel, T., Wolf, B., Benny, O., Rooney, A.G., Ffrench-Constant, C., Enikolopov, G., and Keshet, E. (2016). VEGF preconditioning leads to stem cell remodeling and attenuates age-related decay of adult hippocampal neurogenesis. Proc. Natl. Acad. Sci. USA *113*, E7828–E7836. https://doi.org/10.1073/pnas.1609592113.

62. Tavazoie, M., Van der Veken, L., Silva-Vargas, V., Louissaint, M., Colonna, L., Zaidi, B., Garcia-Verdugo, J.M., and Doetsch, F. (2008). A specialized vascular niche for adult neural stem cells. Cell Stem Cell *3*, 279–288. https://doi.org/10.1016/j.stem.2008.07.025.

63. Telley, L., Govindan, S., Prados, J., Stevant, I., Nef, S., Dermitzakis, E., Dayer, A., and Jabaudon, D. (2016). Sequential transcriptional waves direct the differentiation of newborn neurons in the mouse neocortex. Science *351*, 1443–1446. https://doi.org/10.1126/science.aad8361.

64. Naik, P.P., Praharaj, P.P., Bhol, C.S., Panigrahi, D.P., Mahapatra, K.K., Patra, S., Saha, S., and Bhutia, S.K. (2019). Mitochondrial Heterogeneity in Stem Cells. Adv. Exp. Med. Biol. *1123*, 179–194. https://doi.org/10.1007/978-3-030-11096-3_11.

65. Mannella, C.A. (2006). Structure and dynamics of the mitochondrial inner membrane cristae. Biochim. Biophys. Acta *1763*, 542–548. https://doi.org/10.1016/j.bbamcr.2006.04.006.

66. Li, D., Xu, M., Wang, Z., Huang, P., Huang, C., Chen, Z., Tang, G., Zhu, X., Cai, M., and Qin, S. (2022). The EMT-induced lncRNA NR2F1-AS1 positively modulates NR2F1 expression and drives gastric cancer via miR-29a-3p/VAMP7 axis. Cell Death Dis. *13*, 84. https://doi.org/10.1038/s41419-022-04540-2.

67. Hofmann, J.J., and Iruela-Arispe, M.L. (2007). Notch signaling in blood vessels: who is talking to whom about what? Circ. Res. *100*, 1556–1568. https://doi.org/10.1161/01.RES.0000266408.42939.e4.

68. Kempermann, G., Song, H., and Gage, F.H. (2015). Neurogenesis in the Adult Hippocampus. Cold Spring Harbor Perspect. Biol. *7*, a018812. https://doi.org/10.1101/cshperspect.a018812.

69. Hochgerner, H., Zeisel, A., Lönnerberg, P., and Linnarsson, S. (2018). Conserved properties of dentate gyrus neurogenesis across postnatal development revealed by single-cell RNA sequencing. Nat. Neurosci. 21, 290–299. https://doi.org/10.1038/s41593-017-0056-2.

70. Benarroch, E.E. (2013). Adult neurogenesis in the dentate gyrus: general concepts and potential implications. Neurology 81, 1443–1452. https://doi.org/10.1212/WNL.0b013e3182a9a156.

71. Kempermann, G., and Gage, F.H. (1998). Closer to neurogenesis in adult humans. Nat. Med. 4, 555–557. https://doi.org/10.1038/nm0598-555.

72. Kornack, D.R., and Rakic, P. (1999). Continuation of neurogenesis in the hippocampus of the adult macaque monkey. Proc. Natl. Acad. Sci. USA 96, 5768–5773. https://doi.org/10.1073/pnas.96.10.5768.

73. Najib, S., Saint-Laurent, N., Estève, J.P., Schulz, S., Boutet-Robinet, E., Fourmy, D., Lättig, J., Mollereau, C., Pyronnet, S., Susini, C., and Bousquet, C. (2012). A switch of G protein-coupled receptor binding preference from phosphoinositide 3-kinase (PI3K)-p85 to filamin A negatively controls the PI3K pathway. Mol. Cell Biol. 32, 1004–1016. https://doi.org/10.1128/MCB.06252-11.

74. Tirupula, K.C., Ithychanda, S.S., Mohan, M.L., Naga Prasad, S.V., Qin, J., and Karnik, S.S. (2015). G protein-coupled receptors directly bind filamin A with high affinity and promote filamin phosphorylation. Biochemistry 54, 6673–6683. https://doi.org/10.1021/acs.biochem.5b00975.

75. Bullitt, E. (1990). Expression of c-fos-like protein as a marker for neuronal activity following noxious stimulation in the rat. J. Comp. Neurol. 296, 517–530. https://doi.org/10.1002/cne.902960402.

76. Miyamae, T., Chen, K., Lewis, D.A., and Gonzalez-Burgos, G. (2017). Distinct Physiological Maturation of Parvalbumin-Positive Neuron Subtypes in Mouse Prefrontal Cortex. J. Neurosci. 37, 4883–4902. https://doi.org/10.1523/JNEUROSCI.3325-16.2017.

77. Rupert, D.D., and Shea, S.D. (2022). Parvalbumin-Positive Interneurons Regulate Cortical Sensory Plasticity in Adulthood and Development Through Shared Mechanisms. Front. Neural Circ. 16, 886629. https://doi.org/10.3389/fncir.2022.886629.

78. Tremblay, R., Lee, S., and Rudy, B. (2016). GABAergic Interneurons in the Neocortex: From Cellular Properties to Circuits. Neuron 91, 260–292. https://doi.org/10.1016/j.neuron.2016.06.033.

79. Sohal, V.S., Zhang, F., Yizhar, O., and Deisseroth, K. (2009). Parvalbumin neurons and gamma rhythms enhance cortical circuit performance. Nature 459, 698–702. https://doi.org/10.1038/nature07991.

80. Calverley, R.K., and Jones, D.G. (1990). Contributions of dendritic spines and perforated synapses to synaptic plasticity. Brain Res. Brain Res. Rev. 15, 215–249. https://doi.org/10.1016/0165-0173(90)90002-6.

81. Geinisman, Y., Morrell, F., and deToledo-Morrell, L. (1989). Perforated synapses on double-headed dendritic spines: a possible structural substrate of synaptic plasticity. Brain Res. 480, 326–329. https://doi.org/10.1016/0006-8993(89)90201-1.

82. Paredes, M.F., Sorrells, S.F., Cebrian-Silla, A., Sandoval, K., Qi, D., Kelley, K.W., James, D., Mayer, S., Chang, J., Auguste, K.I., et al. (2018). Does Adult Neurogenesis Persist in the Human Hippocampus? Cell Stem Cell 23, 780–781. https://doi.org/10.1016/j.stem.2018.11.006.

83. Goyal, M.S., Hawrylycz, M., Miller, J.A., Snyder, A.Z., and Raichle, M.E. (2014). Aerobic glycolysis in the human brain is associated with development and neotenous gene expression. Cell Metabol. 19, 49–57. https://doi.org/10.1016/j.cmet.2013.11.020.

84. Beckervordersandforth, R., Ebert, B., Schäffner, I., Moss, J., Fiebig, C., Shin, J., Moore, D.L., Ghosh, L., Trinchero, M.F., Stockburger, C., et al. (2017). Role of Mitochondrial Metabolism in the Control of Early Lineage Progression and Aging Phenotypes in Adult Hippocampal Neurogenesis. Neuron 93, 1518. https://doi.org/10.1016/j.neuron.2017.03.008.

85. Zheng, X., Boyer, L., Jin, M., Mertens, J., Kim, Y., Ma, L., Ma, L., Hamm, M., Gage, F.H., and Hunter, T. (2016). Metabolic reprogramming during neuronal differentiation from aerobic glycolysis to neuronal oxidative phosphorylation. Elife 5, e13374. https://doi.org/10.7554/eLife.13374.

86. Robertson, S. (1993). X-Linked Otopalatodigital Spectrum Disorders. In GeneReviews((R)), M.P. Adam, G.M. Mirzaa, R.A. Pagon, S.E. Wallace, L.J.H. Bean, K.W. Gripp, and A. Amemiya, eds.

87. Sasaki, E., Byrne, A.T., Phelan, E., Cox, D.W., and Reardon, W. (2019). A review of filamin A mutations and associated interstitial lung disease. Eur. J. Pediatr. 178, 121–129. https://doi.org/10.1007/s00431-018-3301-0.

88. Savoy, R.M., and Ghosh, P.M. (2013). The dual role of filamin A in cancer: can't live with (too much of) it, can't live without it. Endocr. Relat. Cancer 20, R341–R356. https://doi.org/10.1530/ERC-13-0364.

89. Lu, J., Lian, G., Lenkinski, R., De Grand, A., Vaid, R.R., Bryce, T., Stasenko, M., Boskey, A., Walsh, C., and Sheen, V. (2007). Filamin B mutations cause chondrocyte defects in skeletal development. Hum. Mol. Genet. 16, 1661–1675.

90. Petersen, P.H., Zou, K., Krauss, S., and Zhong, W. (2004). Continuing role for mouse Numb and Numbl in maintaining progenitor cells during cortical neurogenesis. Nat. Neurosci. 7, 803–811. https://doi.org/10.1038/nn1289.

STAR★METHODS

KEY RESOURCES TABLE

REAGENT or RESOURCE	SOURCE	IDENTIFIER
Antibodies		
NeuN, Clone A60	Millipore	Cat# MAB377 RRID: AB_2298772
NeuN	Cell Signaling Technology	Cat# 24307 RRID: AB_2651140
GFAP	Abcam	Cat# ab7260 RRID: AB_305808
GFAP (GA5)	Novus Biologicals	Cat# NBP2-29415; RRID: AB_2631231
GFAP	Dako (Agilent)	Cat# GA52461-2; RRID: AB_2811722
Cux1	Santa Cruz	Cat# sc-13024; RRID: AB_2261231
Ki67	Dako (Agilent)	Cat# A0047, RRID: AB_2314699
DCX	Abcam	Cat# ab18723; RRID: AB_732011
Sox10	Abcam	Cat# ab227680; RRID: AB_2927464
Olig2	Abcam	Cat# ab109186; RRID: AB_10861310
Col4	Abcam	Cat# ab6586; RRID: AB_305584
Complex I, 75 kD	Millipore	Cat# ABN302; RRID: AB_2915902
Cox4	Proteintech	Cat# 11242 RRID: AB_2085278
PGC1α	Novus Biologicals	Cat# NBP1-04676; RRID: AB_1522118
Atg5	Cell Signaling Technology	Cat# 12994; RRID: AB_2630393
LC3B	Novus Biologicals	Cat# NB100-2220; RRID: AB_10003146
NeuroD2	Abcam	Cat# ab104430; RRID: AB_10975628
Parvalbumin	Sigma	Cat# SAB4200545 RRID: AB_2857970
CAMK2	Proteintech	Cat# 13730-AP; RRID: AB_2070320
CAMK2	R&D systems	Cat# MAB7280; RRID: NA
c-Fos	Novus Biologicals	Cat# NB110-75039; RRID: AB_1048550
GAD 65/67	Sigma	Cat# G5163; RRID: AB_477019
MAP2	Novus Biologicals	Cat # NB120-11268 RRID: AB_791184
CD31	Proteintech	Cat # 28083-1-AP; RRID: AB_2881055
Filamin A	Abcam	Cat# ab76289; RRID: AB_1523618
Filamin B	Santa Cruz	sc376241 RRID: AB_10988205
NCID	Cell Signaling Technology	Cat# 3439; RRID:AB_2153348
Grm1	Boster	Cat# A03049; RRID: AB_3081606
SNAI1	Proteintech	Cat# 13099-1-AP; RRID: AB_2191756
pAMPK	Cell Signaling Technology	Cat# 2535; RRID: AB_331250
pGsk3β	Cell Signaling Technology	Cat# 9336; RRID: AB_331405
Gsk3β	Cell Signaling Technology	Cat# 12456; RRID: AB_2636978
β-Arrestin 1/2	Cell Signaling Technology	Cat# 4674; RRID: AB_10547883
pCREB	Cell Signaling Technology	Cat# 9196; RRID: AB_331275
Calbindin	ThermoFisher	Cat# PA5-85669; RRID: AB_2792808
GAPDH	Sigma	Cat# G9295; RRID: AB_1078992
Actin	Sigma	Cat# A2668; RRID: AB_258014
Tubulin, alpha, clone B-5-1-2	Sigma	Cat# T6074; RRID: AB_477582

Continued

REAGENT or RESOURCE	SOURCE	IDENTIFIER
Vinculin	Sigma	Cat# V9131; RRID: AB_477629
Tuj1	BioLegend	Cat # 801213; RRID: AB_2728521
NeuN, Alexa Fluor 647 conjugated	Cell Signaling Technology	Cat# 62994; RRID: NA
Gfap (GA-5), Alexa Fluor 532 conjugated	Novus	Cat# NBP2-33184AF532; RRID: NA
β-Catenin	BD Biosciences	*Cat# 610154; RRID:* AB_397555
Chemicals, peptides, and recombinant proteins		
Formaldehyde, EM grade	Ted Pella	Cat# 18505
Glutaraldehyde, EM grade	Ted Pella	Cat# 18421
cOmplete™, Mini, EDTA-free Protease Inhibitor Cocktail	Roche	Cat# 11836170001
Leupeptin	ThermoFisher	Cat# 78435
Pepstatin A	ThermoFisher	Cat# 78436
Aprotinin	Sigma	Cat# A6103
Benzamidine	Sigma	Cat# 434760
Phenylmethanesulfonyl fluoride	Sigma	Cat# P7626
Antigen unmasking solution	Vector Lab	Cat# H-3300
Critical commercial assays		
FD Rapid GolgiStain kit	FD Neuro Technologies	Cat # PK401
Click-iT™ Plus EdU Cell Proliferation Kit for Imaging, Alexa Fluor™ 488 dye	ThermoFisher	Cat# C10637
Click-iT™ Plus EdU Cell Proliferation Kit for Imaging, Alexa Fluor™ 555 dye	ThermoFisher	Cat# C10638
Deposited data		
GeoMx DSP of mouse whole transcriptome	This work	GEO: GSE256342
Experimental models: Organisms/strains		
Flna floxed mice	in house (Feng et al., 2006[55])	https://www.pnas.org/doi/abs/10.1073/pnas.0609628104?url_ver=Z39.88-2003&rfr_id=ori%3Arid%3Acrossref.org&rfr_dat=cr_pub++0pubmed
Flnb KO mice	in house (Lu et al., 2007[89])	https://pubmed.ncbi.nlm.nih.gov/17510210/
Emx1 Cre mice	JaxMice	Strain # 005628
Nes8 Cre mice Tg (Nes-cre)1Wmz	in house (Petersen et al., 2002)	https://pubmed.ncbi.nlm.nih.gov/12410312/
Software and algorithms		
Image-Pro Premier	Media Cybernetics	https://www.mediacy.com/support/imagepropremier
NIH Image J	ImageJ	https://imagej.nih.gov/ij/
GraphPad Prism 10	GraphPad	https://www.graphpad.com/scientific-software/prism/
Microsoft Office Excel	Microsoft	https://www.microsoft.com
R studio	R Studio 2020 Team	http://www.rstudio.com/
DAVID (The Database for Annotation, Visualization and Integrated Discovery, web tool)	NIH DAVID Bioinformatics	https://david.ncifcrf.gov/
ShinyGO v0.741 Gene Ontology Enrichment Analysis (web tool)	Ge et al., Bioinformatics 2020	http://bioinformatics.sdstate.edu/go74/

(Continued on next page)

Continued

REAGENT or RESOURCE	SOURCE	IDENTIFIER
Metascape (web tool)	Zhou et al. Zhou et al. Nature Commun. 2019	https://metascape.org/gp/index.html#/main/step1
PANTHER 18.0 (web tool)	Mi et al., NA 2013	https://www.pantherdb.org/
MORPHEUS (web tool)	Starruß et al., Bioinformatics 2014	https://software.broadinstitute.org/morpheus/

RESOURCE AVAILABILITY

Lead contact

Further information and requests for resources and reagents should be directed to and will be fulfilled by the Lead Contact, Yuanyi Feng (yuanyi.feng@usuhs.edu).

Materials availability

All the materials generated in this study are available upon reasonable request to the lead contact.

Data and code availability

- GeoMx Digital Spatial Profiling dataset has been deposited in NCBI's Gene Expression Omnibus (GEO): GSE256342 and is publicly accessible.
- This paper does not report original code.
- Any additional information required to reanalyze the data reported in this paper is available from the lead contact upon request.

EXPERIMENTAL MODEL AND STUDY PARTICIPANT DETAILS

Mice

Flna floxed (Flna$^{flox/flox}$ female or Flna$^{flox/y}$ male) mice, and Flnb knockout mice (Flnb$^{-/-}$) were generated by conventional mouse embryonic stem cell-based gene targeting.[55,89] NSPC-specific Flna conditional knockout mice were generated by crossing Flna$^{flox/flox}$ mice with Tg(Nes-Cre)1Wmz Cre mice.[90] The Flna;Flnb compound mutant mice were generated by standard genetic cross. Male and female mice from embryonic day 14.5 (E14.5) to 10 months of age were analyzed. All mice used for this study were housed and bred in compliance with the AAALAC's guidelines according to animal study protocols BIO-17-024, BIO-20-018, BIO-21-024, and BIO-23-143 that were approved by the IACUC committees of Uniformed Services University of Health Services. Experiments were performed using littermates or age and genetic background matched control and mutant groups in both sexes.

METHOD DETAILS

Fluorescence immunohistological and immunochemical analyses

For immunofluorescence staining of mouse cortical tissue, mouse brains were fixed by transcardial perfusion with PBS and 4% paraformaldehyde and then processed in 12um cryosections or 5 um paraffin sections. After treating with antigen unmasking solutions (Vector Labs), brain sections were blocked with 5% goat serum and incubated with primary antibodies in PBS, 0.05% Triton X100, and 5% goat serum at 4°C overnight, and followed by staining with fluorescence conjugated antibodies and Hoechst 33342. Epifluorescence images were acquired with a Leica CTR 5500 fluorescence, DIC, and phase contrast microscope equipped with the Leica DFC7000T digital camera. Images were imported to Adobe Photoshop and adjusted for brightness and black values.

GeoMx Digital Spatial Profiling of the mouse whole-transcriptome

Preparation of samples for full transcriptome spatial RNA-seq analysis was carried out following the GeoMx DSP slide preparation user manual (MAN-10150). Briefly, brains of three Fln^{KO} and three control mice at 3 months of age were fixed by transcardial perfusion with nuclease-free PBS and 4% paraformaldehyde. From the fixed brains cryosections of 7-µm thickness were placed on a microscope slide. The slide was incubated with mouse whole transcriptome oligonucleotide probe mix overnight, then washed and stained with Alexa Fluo 647 conjugated antibody to NeuN (Cell Signaling Technology), Alexa Fluo 532 conjugated antibody to Gfap, (Novus Biologicals), and DNA dye Syto13. Tissue sections were then loaded into the GeoMx DSP platform by which immunofluorescence signals were visualized by three colors (Green = Gfap; Red = NeuN; blue = Syto13) for selecting Regions-Of-Interests (ROIs). Circular geometric ROIs of ~100um in diameter were selected from V-SVZ or upper cortical layers of control and Fln^{KO} brains, as well as periventricular nodules of Fln^{KO} brains. Oligonucleotide probes in each ROI were released by UV light and collected in separate wells of a microtiter plate. Photo-released nucleotides were used to generate sequencing libraries by PCR, during which Illumina i5 and i7 dual-indexing primers were added to uniquely index each ROI. PCR reactions were purified by AMPure beads twice. Library concentration was determined by a Qubit fluorometer and libraries

were paired-end sequenced on a NextSeq 500 system (Illumina). The sequencing results were processed through standard GeoMx NGS Pipeline according to GeoMx DSP NGS Readout User Manual (MAN-10153-01), during which raw sequencing FASTQ files were converted to digital count conversion (DCC) files and further processed to obtain data for each target probe in each ROI by subtracting the mean of background and normalizing to Q3 of all targets. The ROIs were categorized according to genotype and spatial groups. Differential gene expression analyses were performed on different groups of ROIs by Student's t test with Benjamini-Hochberg adjustment. Adjusted p values of < 0.05 were regarded significant.

Ultra-structural analysis

Mouse brains were fixed with EM grade formaldehyde (2%) and glutaraldehyde (2%) in PBS by transcardial perfusion. The neocortex and V-SVZ of perfused brains were dissected, cut to pieces of < 1 mm^3 in size, immersed in the same fixative overnight, and washed three times in PBS. Samples were then washed 3x 15min in cacoldylate buffer (CB, 0.1M, pH 7.4) to remove phosphate ions and subsequently immersed in 2% OsO$_4$ in CB for 1 hour. Following 3x15 min washes in CB, samples were dehydrated in a graduated series of ethanol, infiltrated with Spurr's epoxy resin (Electron Microscopy Sciences, Hatfield, PA), and polymerized at 70°C for 10 hours. Thin sections (70-90nm) were cut on a Leica Ultracut UC-6 ultramicrotome (Leica Microsystems, Wetzlar, Germany). Sections were collected on 3mm copper grids and subsequently stained for 30min with 2% aqueous uranyl acetate and for 5min with Reynold's lead citrate. The stained brain specimens were examined with a JEOL JEM-1011 transmission electron microscope. Images were acquired by an Advanced Microscopy Techniques 4MP digital camera (AMT Corp) and saved as TIFF files. Mitochondria quantification was performed by manually tracing the outer mitochondrial membrane using ImageJ.

Golgi-Cox staining for neuronal morphology and dendritic spine analysis

Mice were euthanized with CO$_2$; brains were quickly dissected, rinsed with deionized water, immersed in impregnation solution, and processed using FD Rapid GolgiStain kit (FD NeuroTechnologies) according to manufacturer's instructions. Stained sections were examined under a Leica DM5000 light microscope. Pyramidal neurons in the cerebral cortex and hippocampus regions were imaged with a 40x objective and photographed. For dendritic spine analyses, 16-20 pyramidal neurons in neocortical layer II/III of each mouse were randomly selected for assessment. The number of spines per 10 micrometers in secondary apical dendrites (branched from primary dendrites arising from the soma), spine length, neck width, head width, and the fraction of spines with doughnut or horseshoe-shaped heads, were scored using the NIH ImageJ and Image-Pro software.

Immunoblotting

Immunoblotting of total cell or tissue proteins was performed by extracting with boiling 2x SDS PAGE sample buffer (62.5 mM Tris-HCl, pH 6.8, 2.5% SDS, 0.7135 M β-mercaptoethanol, 10% glycerol, 0.002% Bromophenol Blue) to fully dissolve the tissue proteins, heating at 95°C for 10 min to ensure protein denaturation, and passing through syringes with a 29-gauge needle three times to sheer nuclear DNA and obtain homogenous extracts. 10-30 ug of total proteins were used for each immunoblotting analysis. The loadings were adjusted and normalized by the total protein content according to Coomassie blue stain of the gel after SDS PAGE and by the level of housekeeping proteins.

QUANTIFICATION AND STATISTICAL ANALYSIS

No statistical methods were used to predetermine sample size, while all experiments were performed with a minimum of three biological replicates and all cell counts were obtained from at least ten random fields. The experiments were not randomized; the investigators were not blinded to the sample allocation and data acquisition during experiments but were blinded in performing quantitative analyses of immuno-histological images using the NIH ImageJ and Image-Pro software. All statistical analyses were done using GraphPad Prism 10.0 software. Data were analyzed by one-way ANOVA or unpaired two-tailed Student's t tests for comparing differences between different genotypes. Differences were considered significant with a p value < 0.05. Data distribution was assumed to be normal but this was not formally tested.